UCRL-JRNL-217559

LAWRENCE
LIVERMORE
NATIONAL
LABORATORY

Piecewise linear discretization of Symbolic Implicit Monte Carlo radiation transport in the difference formulation

E. D. Brooks III, A. Szoke, J. D. L. Peterson

December 6, 2005

Disclaimer

This document was prepared as an account of work sponsored by an agency of the United States Government. Neither the United States Government nor the University of California nor any of their employees, makes any warranty, express or implied, or assumes any legal liability or responsibility for the accuracy, completeness, or usefulness of any information, apparatus, product, or process disclosed, or represents that its use would not infringe privately owned rights. Reference herein to any specific commercial product, process, or service by trade name, trademark, manufacturer, or otherwise, does not necessarily constitute or imply its endorsement, recommendation, or favoring by the United States Government or the University of California. The views and opinions of authors expressed herein do not necessarily state or reflect those of the United States Government or the University of California, and shall not be used for advertising or product endorsement purposes.

Piecewise linear discretization of Symbolic Implicit Monte Carlo radiation transport in the difference formulation *

Eugene D. Brooks III *, Abraham Szőke, Jayson D. L. Peterson

University of California, Lawrence Livermore National Laboratory,
P.O. Box 808, Livermore, CA 94550, USA

Abstract

We describe a Monte Carlo solution for time dependent photon transport, in the difference formulation with the material in local thermodynamic equilibrium (LTE), that is piecewise linear in its treatment of the material state variable. Our method employs a Galerkin solution for the material energy equation while using Symbolic Implicit Monte Carlo (SIMC) to solve the transport equation. In constructing the scheme, one has the freedom to choose between expanding the material temperature, or the equivalent black body radiation energy density at the material temperature, in terms of finite element basis functions. The former provides a linear treatment of the material energy while the latter provides a linear treatment of the radiative coupling between zones. Subject to the conditional use of a lumped material energy in the vicinity of strong gradients, possible with a linear treatment of the material energy, our approach provides a robust solution for time dependent transport of thermally emitted radiation that can address a wide range of problems. It produces accurate results in the diffusion limit.

Key words: difference formulation, radiation transport, implicit Monte Carlo

1   Introduction

In earlier work, [1] and [2], some of the authors introduced the difference formulation for photon transport, under conditions of local thermodynamic equilibrium (LTE) for the material, and demonstrated a significant gain in computational efficiency for a Symbolic Implicit Monte Carlo (SIMC) [3] [4] implementation that assumes a constant material temperature in a zone. In order to obtain accurate results, the zone size for this piecewise constant implementation is limited to about one mean free path. The cause of this limitation is energy teleportation [5], wherein energy that is absorbed on one side of a zone is immediately re-emitted on the opposite side. This defect causes a faster-than-physical propagation velocity for a Marshak (thermal) wave, and excessive energy transport even under steady state conditions.

Clouet and Samba [6] have shown that a piecewise linear (in space) discretization of the material state variable produces the correct diffusion limit. They did this in the context of a linearized form of the transport problem for a time independent solution; see [7] for an example of this linearization in a diffusion context. As they used the standard formulation of transport, Monte Carlo noise was an issue that led them to the conclusion that practical application of the method might be limited by the noise problem.

The method of Clouet and Samba is based on a Galerkin [8] solution of the material energy equation and uses a piecewise linear finite element basis that permits discontinuities at interior zone edges in order to represent the material state variable within a zone. In this paper, we extend the method of Clouet and Samba to the time dependent solution of the full non-linear equations of LTE transport in the difference formulation, using piecewise linear basis functions, in slab geometry.

A significant difficulty that occurs in the standard formulation of transport when attempting to extend SIMC with a finite element treatment of the material state variable is that of correctly sampling the source term. Correct sampling of the emission spectrum, when it depends upon the details of the material opacity at the temperature of the position sampled, requires an integral of the opacity against the Planck distribution function for each particle sampled. In the difference formulation, the thermal emission in a zone does not depend on the material opacity and this difficulty does not occur.

In addressing the non-linear equations of time dependent radiation transport, one has a choice between representing the temperature, T, or the equivalent black body radiation energy density at the material temperature, $\Phi = aT^4$, using finite element basis functions. In the former, the material energy is linear when a constant specific heat is used during a time step while the radiative

coupling between zones is not. In the latter, the radiative coupling between zones is linear while the material energy, expressed in terms of Φ, is not. The best choice depends whether the problem of interest contains violent time dependent behavior or more closely resembles steady state conditions.

A time dependent finite element (piecewise linear) solution of radiation transfer becomes non-monotonic in the vicinity of a strong gradient. When a thermal wave impinges on one side of an optically thick zone, the self consistent solution of the energy equation drives the far side down in temperature, even though the energy absorbed is positive (but small). This problem becomes particularly serious when the initial temperature of the material is small, as it can lead to negative temperature excursions that stop the calculation. The problem, analyzed by Godunov [9] in the context of fluid flow, is unavoidable in linear schemes that achieve second order accuracy. The technique of lumping the material energy (or mass) matrix [8] is a method used to address this problem in conventional applications of the finite element method. We find lumping to be a useful means of avoiding the monotonicity problem in the context of transport for thermally emitted photons. However, lumping reduces the accuracy of the solution in the affected zones. It gets the average temperature correct, but introduces an error in the slope of the solution that would otherwise be second order accurate.

In Section 2 we briefly describe the difference formulation for the transport of photons, under conditions of local thermodynamic equilibrium, in the slab geometry environment that we will use for our exposition in this paper. In Section 3, we sketch the solution method, and refer to other sections of the paper that provide extensive details of the implementation. We provide numerical results in Sections 8 and 9, documenting the characteristics of the method for problems involving an optical thickness of one mean free path per zone. In Section 11 we demonstrate the performance of the method for a thermal wave penetration problem that is optically thick, comparing its behavior to that of the piecewise constant treatment of the material state variable. We provide a discussion in Section 12. The intervening sections and Appendices of this paper delve into the significant details of our method.

2   The difference formulation

We want to solve the coupled equations for photon transport, Eq. (1), and the material energy, Eq. (2), in the difference formulation. In this model for photon transport the interaction of the radiation with the material (absorption and thermal emission) is accomplished using the simplifying assumption of local thermodynamic equilibrium (LTE) for the material degrees of freedom. For the purposes of this paper we restrict the problem to slab geometry, ex-

clude physical scattering, and assume that the material is stationary. Lifting these restrictions poses no significant difficulties for the Monte Carlo solution method we describe. We have exposed the independent variables in the equations below for clarity.

$$\frac{1}{c}\frac{\partial D(x,t;\nu;\mu)}{\partial t} + \mu\frac{\partial D(x,t;\nu;\mu)}{\partial x} = -\sigma'_a(\nu,T(x,t))D(x,t;\nu;\mu)$$
$$-\frac{1}{c}\frac{\partial B(\nu,T(x,t))}{\partial t} - \mu\frac{\partial B(\nu,T(x,t))}{\partial x} \quad (1)$$

$$\frac{\partial E_{mat}(T(x,t))}{\partial t} = 2\pi\int_0^\infty d\nu\int_{-1}^1 d\mu\,\sigma'_a(\nu,T(x,t))D(x,t;\nu;\mu) + G(x,t) \quad (2)$$

The field that is transported, D, is the difference between the specific intensity for photons, I, and the black body distribution at the material temperature, $B(\nu,T(x,t))$; that is $I = D + B$ provides the relationship between the difference formulation and the standard formulation for photon transport with the material in LTE. It also provides a means for mapping boundary conditions between the two formulations. It is useful to note that the opacity corrected for stimulated emission, σ'_a, the material energy, E_{mat}, and the local blackbody field, B, are indirect functions of space and time through their dependence on the temperature, $T(x,t)$. This becomes important when the temperature, $T(x,t)$, is a function of space, and possibly time, during a time step.

We define the black body radiation energy density, $\Phi = aT^4$, where a is the radiation constant. The factorization of B into a strength times a frequency distribution function gives

$$B(\nu,T) = \frac{c\,a\,T^4}{4\pi}\,b(\nu,T)\quad, \quad (3)$$

with

$$\int_0^\infty b(\nu,T)d\nu = 1\quad, \quad b(\nu,T) > 0\quad. \quad (4)$$

Equivalently, one can express B in terms of Φ,

$$B(\nu,\Phi) = \frac{c\,\Phi}{4\pi}\,b(\nu,\Phi)\quad. \quad (5)$$

The source terms in the radiation transport equation for the difference field, D, can be factored using the chain rule, giving

$$-\frac{1}{c}\frac{\partial B}{\partial t} - \mu\frac{\partial B}{\partial x} = \frac{4\pi}{c}\frac{\partial B}{\partial \Phi}\left[-\frac{1}{4\pi}\frac{\partial \Phi(x,t)}{\partial t} - \frac{\mu c}{4\pi}\frac{\partial \Phi(x,t)}{\partial x}\right] \quad . \tag{6}$$

The use of the chain rule to factor the source terms in the difference formulation is the equivalent of the factorization of the Planck distribution, Eq. (3), used in the standard formulation of SIMC transport. The term $(4\pi/c)(\partial B/\partial \Phi)$ is a frequency distribution function, it is positive and its frequency integral is unity. The sampling of this frequency distribution was dealt with in detail in the Appendix of [2] and is further refined for the finite difference case in the Appendix of this paper.

3   Solution Method

The sections that follow contain a detailed account of the implementation of our solution of Eqs. (1) and (2), using a SIMC method that employs a piecewise linear finite element treatment of the material state variable. Our method is similar to that of Clouet and Samba [6]. In a nutshell, our algorithm is organized as follows:

- The material state variable is represented with a finite element expansion in space. The time dependence is given by the time dependence of the expansion coefficients.
- The source terms of the transport equation, which depend only upon the material state variable and no other physical properties, are worked out in terms of space, angle, and frequency distributions that are known at the beginning of the time step and in terms of a strength that depends upon coefficients of the finite element expansion that will not be known until the end of the time step.
- The source terms are sampled and the transport equation is solved by a Monte Carlo simulation that propagates these sources, which carry the unknown strength terms symbolically, along with any census particles, which hold known weights from a prior time step, to the end of the current time step.
- The equation for the change to the material energy is solved by using a Galerkin [8] projection to produce a set of equations that relate the unknown coefficients of the finite element expansion for the material state variable.
- The set of equations for the material state variable is solved, and the solution is then used to resolve the unknown factors in the census particle list in order to prepare the initial conditions for the next time step.

5

In addition to the finite element basis employed by Clouet and Samba that admits discontinuities at the interfaces of interior zones, we also demonstrate a modification of this basis that enforces continuity of the solution on interior zone interfaces. The finite element basis we use is described in Section 4.1 and our method of collapsing to a basis that enforces continuity is described in Section 10.

We use an implicit piecewise constant time discretization for most of this paper. The implicit treatment is required in order to obtain unconditional stability of the resulting numerical method. We have also implemented an implicitly interpolated piecewise linear time discretization and find it to be conditionally stable. This time discretization might be used in order to obtain faster convergence as a function of the size of the time step, with due caution with regard to the treatment of material properties such as opacity and specific heat. Our scheme for time discretization is described in Section 4.2.

The underlying SIMC method is based on the idea of factoring the source terms into space, time and frequency distributions that are known at the beginning of the time step, and strength that depends upon the radiation energy density, $\Phi = aT^4$, or temperature, T, as the case may be, that will not be known until the end of the time step. This allows the source terms to be sampled in space, time, and frequency while leaving the weights of the Monte Carlo particles unknown. The transport equation is then solved in terms of the unknown values of the material state variable by Monte Carlo simulation. The source particle sampling in this paper is substantially complicated by the piecewise linear treatment of the material state variable. This is described at length in Section 6 as well as in the Appendix.

As the Monte Carlo particles propagate they lose their energy to the matter. This energy deposition, along with material energy and heating terms, must be accounted for in the solution of the material energy equation. Some of the terms that appear in the energy equation are non-linear, as a function of space, and this forces us to resort to the Galerkin method in order to solve for the material state variable at the end of the time step. In the Galerkin method, a set of algebraic equations for the material state variable is generated by projecting the material energy equation on the basis functions. By using this solution strategy, we restrict the solution for the material state variable to be a member of the space of functions spanned by the piecewise linear basis. This is discussed in Section 7.

The set of algebraic equations produced by the Galerkin projection of the energy equation is non-linear in the unknown coefficients of the finite element expansion for the material state variable at the end of the time step. We resort to Newton-Raphson iterations to solve this set of equations, employing the known material state values at the start of the time step as the starting

point. For each iteration of the solver, the Newton-Raphson solution of the energy equation requires the Galerkin projection of the energy equation and its partial derivatives with respect to the unknown material state variable. The partial derivatives are evaluated analytically, instead of numerically, and the consistency of the Galerkin projection and its partial derivatives is of paramount importance to the robustness of the solver. Although we do not document these issues completely, enough key details are described in Section 7 that our results may be reproduced.

Once the solution for the material state variable is known, the unknown factors for the weights of Monte Carlo particles born during the time step are determined and the census particle list is converted to numeric weights in order to form the initial condition for the transport equation during the next time step.

4   The basis functions

In our piecewise linear Symbolic Implicit Monte Carlo solution in the difference formulation, we use piecewise linear basis functions to handle the spatial discretization of the material state variable. The spatial basis functions, permitting discontinuity at zone boundaries, are the same as those that were employed by Clouet and Samba [6] in their linearized treatment of the transport equation. We have explored the addition of temporal basis functions in an attempt to extend the second order accurate treatment to the time variable, but find that the result is only conditionally stable. Later on in our discussion, we will describe how to constrain the solution of the material energy equation so that continuity is preserved at interfaces between interior zones.

4.1   Spatial discretization

We write out the piecewise linear basis functions, supporting discontinuities at zone edges, in slab geometry, in order to establish our notation. Extension to two and three dimensional geometry is straightforward, as described by Clouet and Samba.

We define N zones, Z_i, $i \in (1, N)$. In each zone there are L basis functions, χ_i^l, $l \in (1, L)$. In slab geometry, $L = 2$. Denoting the left and right boundaries of Z_i by x_i and x_{i+1} respectively, the basis functions for slab geometry are

defined as:

$$
\chi_i^1(x) = \begin{cases} 0 & (x < x_i) \\ \dfrac{x_{i+1} - x}{x_{i+1} - x_i} & (x_i \le x \le x_{i+1}) \\ 0 & (x_{i+1} < x) \end{cases} \quad , \tag{7}
$$

$$
\chi_i^2(x) = \begin{cases} 0 & (x < x_i) \\ \dfrac{x - x_i}{x_{i+1} - x_i} & (x_i \le x \le x_{i+1}) \\ 0 & (x_{i+1} < x) \end{cases} \quad . \tag{8}
$$

It is easy to see that

$$
\sum_{l=1}^{L} \chi_i^l(x) = 1 \quad (x_i \le x \le x_{i+1}) \quad , \tag{9}
$$

and is zero otherwise. The fact that the basis functions add up to one within each zone is important for energy conservation, and can be exploited when sampling although we do not do so.

Defining

$$
\overline{\chi}_i^l(x) = (2/(x_{i+1} - x_i))\chi_i^l(x) \quad , \tag{10}
$$

we produce a normalized basis function with unit integral. This version of the basis function is useful when decomposing source terms for the purpose of Monte Carlo sampling. The concept will be extended to cover products of basis functions later on.

It is sometimes useful to organize things in terms of the zone edges, x_i, $i \in (1, N + 1)$, which are located at the left and right edges of the zones, Z_i, $i \in (1, N)$. We will be careful to point out when we do so.

A function, $F(x, t)$, that is piecewise linear in each zone, can be represented in terms of the spatial basis functions by the expansion

$$
F(x, t) = \sum_{i=1}^{N} F_i(x, t) = \sum_{i=1}^{N} \sum_{l=1}^{L} F_i^l(x, t) = \sum_{i=1}^{N} \sum_{l=1}^{L} f_i^l(t) \chi_i^l(x) \quad . \tag{11}
$$

The expansion permits discontinuity in $F(x)$ at the internal interfaces between

zones as there is no constraint relating f_i^2 and f_{i+1}^1. If $F(x)$ is continuous on the zone boundaries, $f_i^2 = f_{i+1}^1$.

4.2 Temporal discretization

In Eq. (11) we defined the spatial discretization method that we employ for the material state variable and, therefore, for the transport source terms, in this paper. The time step is the interval between t_0 and $t_0 + \Delta t$. The temporal discretization is defined in how we treat the time dependence of the coefficients, $f_i^l(t)$. The first possibility, which we call *explicit*, is for $f_i^l(t)$ to equal $f_i^l(t_0)$ during the duration of the time step from t_0 to $t_0 + \Delta t$, and then abruptly change to $f_i^l(t_0 + \Delta t)$ at the end. A second possibility, which we call *implicit*, is for $f_i^l(t)$ to abruptly change from $f_i^l(t_0)$ to $f_i^l(t_0 + \Delta t)$ at the beginning of the time step, maintaining this value until the end.

A third possibility is that the $f_i^l(t)$ vary linearly across the time step, which we call *interpolated*. To this end, we define the functions $\alpha(t)$ and $\beta(t)$,

$$\alpha(t) = \frac{t_0 + \Delta t - t}{\Delta t} \quad (t_0 < t < t_0 + \Delta t), \quad = 0 \text{ (otherwise)} \quad , \tag{12}$$

and

$$\beta(t) = \frac{t - t_0}{\Delta t} \quad (t_0 < t < t_0 + \Delta t), \quad = 0 \text{ (otherwise)} \quad . \tag{13}$$

The interpolated representation of $f_i^l(t)$ can now be expanded in terms of the temporal basis functions.

$$f_i^l(t) = f_i^l(t_0)\alpha(t) + f_i^l(t_0 + \Delta t)\beta(t) \tag{14}$$

By expanding $f_i^l(t)$ in terms of the temporal basis functions we interpolate between the known value, $f_i^l(t_0)$, at the beginning of the time step and the unknown value, $f_i^l(t_0 + \Delta t)$, at the end of the time step. The result is an implicit second order treatment of the time dependence of $f_i^l(t)$.

The explicit temporal treatment was explored in [10] for the difference formulation of a linear transport problem, and found to be conditionally stable in an environment where the spatial treatment of the material state variable was constant in a zone. We will not discuss explicit temporal treatment in this paper. The implicit treatment was explored in [2] for the difference formulation of radiation transport in LTE using a constant material temperature (as a function of space) in a zone. It was found to be unconditionally stable in

practice. We will explore the implicit temporal treatment, using the piecewise linear spatial discretization, in this paper. The interpolated temporal treatment offers the possibility of second order accuracy for the time integration as a complement to the second order accuracy that we obtain from the piecewise linear basis functions used for the spatial discretization. We have only briefly explored the interpolated temporal treatment, finding numerical evidence for conditional stability. A detailed stability analysis is postponed to future work.

5   The solution of the transport equation

We employ the Symbolic Implicit Monte Carlo (SIMC) technique [3] to produce a statistical sample of the solution to the transport equation that depends upon the unknown coefficients in the expansion of the material state variable at the end of the time step. Either a finite element expansion for the material temperature, $T(x, t)$, or for the black body radiation energy density at the material temperature, $\Phi(x, t) = aT^4$, can be used to construct the source terms of the transport equation. In either case, the sources are sampled statistically as Monte Carlo particles and Eq. (1) is solved by propagating the particles.

As shown in Eq. (6), the source terms for the transport equation can be factored using the chain rule, cleanly separating the frequency dependence from the strength of the sources. We would like to note that it is important to factor out the frequency dependence before decomposing the strength terms for the purpose of Monte Carlo sampling. By doing this, all particles born at a given space and time point can be sampled from the same frequency distribution.

Important assumptions of the scheme are that: the frequency distribution of thermally emitted photons, the absorption coefficients of photons as they traverse the time step, and any scattering coefficients, are all functions of space and time that are determined from information known at the beginning of the time step. We would like to note that stimulated (e.g. Compton) scattering is not consistent with these assumptions, with enhancements of the scattering coefficient being dependent upon the strength of the radiation field in the direction and frequency being scattered into. One must face this issue when considering practical applications of our method, but we ignore it for now.

In addition to the "symbolic" source terms in the transport equation, there are the initial conditions for each time step (the census photons left from the previous time step), and the possibility of prescribed sources of Monte Carlo particles from the boundary conditions. Unlike the sources associated with the $\partial \Phi / \partial t$ and $\partial \Phi / \partial x$ terms in Eq. (6), these sources have numeric weights with known factors. Using these sources, the exact initial and boundary conditions

10

for the transport problem are rigorously satisfied.

Under the assumptions noted above, the radiation transport equation for the time step, derived from Eq. (1), is linear in its sources. Therefore the source terms may be decomposed in ways that are advantageous for sampling, or for dealing with cancellations that would otherwise produce noise. In fact, the linearity of the transport equation for the time step, with respect to its sources and initial conditions, is essential to achieving the goal of running the Monte Carlo in a single pass (or at all).

6   Monte Carlo sampling the source terms

In extending the Symbolic Implicit Monte Carlo method to a finite element treatment of the material energy equation, we are free to choose between expanding $\Phi(x, t) = aT^4$ or the material temperature, $T(x, t)$, in the basis functions. Examining Eq. (6), the advantage of expanding Φ becomes clear. With this choice the source terms are linear in Φ and this greatly simplifies the task of Monte Carlo sampling. It also makes the radiative couplings between zones linear. In a thick system with constant opacity near a steady state, this choice for expanding the material state variable approaches the exact solution. The disadvantage of expanding Φ, even for a constant material specific heat, is that the expression for the material energy is made non-linear. This problem becomes significant when one needs to lump the material energy in order to prevent negative excursions of the material state variable in the presence of steep gradients.

The alternative, expanding the material temperature, $T(x, t)$, in the linear basis functions, has its own advantages and disadvantages. The treatment of the material energy becomes linear, enabling lumping and straightforward coupling to other physics that treats the material temperature similarly. On the other hand, Monte Carlo sampling of the source terms is more complicated and the radiative coupling between zones becomes non-linear. We explore both approaches in our investigation, evaluating each one on its merits.

6.1   Expanding Φ in the finite element basis functions

Expanding $\Phi(x, t) = aT^4$ in the basis functions provides the simplest Monte Carlo implementation of the source terms.

$$\Phi(x, t) = \sum_{i=1}^{N} \Phi_i(x, t) = \sum_{i=1}^{N} \sum_{l=1}^{L} \Phi_i^l(x, t) = \sum_{i=1}^{N} \sum_{l=1}^{L} \phi_i^l(t) \chi_i^l(x) \qquad (15)$$

11

In our detailed exposition of the Monte Carlo sampling of the source terms we assume the piecewise constant (in time) *implicit* temporal discretization described in Section 4.2 where the $\phi_i^l(t)$ abruptly jump to their end of time step values, $\phi_i^l(t_0 + \Delta t)$, immediately after the beginning of the time step.

We now use the spatial expansion of Φ defined in Eq. (15), the definition of the strength of the source terms from Eq. (6) after factoring out the frequency distribution function given by $(4\pi/c)(\partial B/\partial \Phi)$, and the above understanding of the temporal treatment, to write down the source terms for the Monte Carlo treatment. First, we deal with the time derivative source.

$$
\begin{aligned}
-\frac{1}{4\pi}\frac{\partial \Phi_i(x,t)}{\partial t} &= -\frac{1}{4\pi}\sum_l \frac{d\phi_i^l(t)}{dt}\chi_i^l(x) \\
&= -\frac{1}{4\pi}\sum_l \delta(t-t_0)(\phi_i^l(t_0+\Delta t)-\phi_i^l(t_0))\chi_i^l(x) \\
&= -\frac{x_{i+1}-x_i}{[2]\times 4\pi}\sum_l [\delta(t-t_0)](\phi_i^l(t_0+\Delta t)-\phi_i^l(t_0))[\overline{\chi}_i^l(x)] \quad (16)
\end{aligned}
$$

The distribution functions for generalized particle coordinates have been denoted by enclosure in [ ]. The angular distribution function, $1/2$, which provides for a uniform distribution for μ in the range $[-1,1]$, is included in the denominator, 8π. There are two spatial distributions for particles born in zone Z_i: those distributed according to $\overline{\chi}_i^1(x)$ and those distributed according to $\overline{\chi}_i^2(x)$. The temporal distribution function is $\delta(t-t_0)$, where δ is the Dirac delta function, indicating that all source particles are born at the beginning of the time step. In our implementation we emit two equally sized samples of M particles in each zone, spatially distributed according to $\overline{\chi}_i^l(x)$ and having a numeric weight $-(x_{i+1}-x_i)/(4\pi M)$. Each particle carries an unknown factor, $(\phi_i^l(t_0+\Delta t)-\phi_i^l(t_0))$, arising from the fact that $\phi_i^l(t_0+\Delta t)$ is not yet known.

The final detail is the frequency distribution for the source particles. As the frequency distribution must be determined before we know $\phi_i^l(t_0+\Delta t)$, we use values extrapolated from past behavior $\widetilde{\phi}_i^l(t_0 + \Delta t)$ in order to construct an estimate for $\Phi_i(x,t_0+\Delta t)$ at the spatial point sampled for each particle. The frequency distribution is the finite difference form of $(4\pi/c)(\partial B/\partial \Phi)$ using $\Phi(x,t_0)$ and $\widetilde{\Phi}(x,t_0+\Delta t)$ evaluated at the point, x, sampled for each particle.

Lacking any constraint enforcing continuity of $\Phi(x,t)$ at the interior zone edges, x_i, $i \in (2,N)$, there are two components associated with the $\partial B/\partial x$ source term. The first is a source of particles emitted *within* zone Z_i, again using the piecewise constant *implicit* time treatment discussed in Section 4.2,

$$-\frac{\mu c}{4\pi}\frac{\partial \Phi_i(x,t)}{\partial x} = -\frac{\mu c}{4\pi}\sum_l \phi_i^l(t)\frac{d\chi_i^l(x)}{dx} = -\frac{\mu c}{4\pi}\frac{\phi_i^2(t) - \phi_i^1(t)}{x_{i+1} - x_i}$$

$$= -\frac{\mu c}{4\pi}\frac{(\phi_i^2(t_0 + \Delta t) - \phi_i^1(t_0 + \Delta t))}{x_{i+1} - x_i}$$

$$= -\frac{[2\mu]c\Delta t}{8\pi}\frac{(\phi_i^2(t_0 + \Delta t) - \phi_i^1(t_0 + \Delta t))}{[\Delta t][x_{i+1} - x_i]} \qquad . \qquad (17)$$

As was discussed in [2], the integral of this source over the range of μ is zero. We deal with this by sampling the range of μ from 0 to 1 and emitting a pair of particles of equal and opposite weight and direction. With that understood, we can read off the distribution functions that have been denoted by enclosure in [ ]. The distribution function for μ is 2μ. The distribution function for the time coordinate is $1/\Delta t$, reflecting a uniform distribution across the interval from t_0 to $t_0 + \Delta t$. The spatial distribution function is $1/(x_{i+1} - x_i)$, reflecting a uniform distribution across zone Z_i. M particle pairs are emitted within each zone, one member of each pair with a numeric weight of $-c\Delta t/8\pi M$ traveling in the positive μ direction, and the other with a weight of opposite sign traveling in the $-\mu$ direction. The particles carry the unknown factor $(\phi_i^2(t_0 + \Delta t) - \phi_i^1(t_0 + \Delta t))$. The frequency of the emitted particles is sampled using the frequency distribution $(4\pi/c)(\partial B/\partial \Phi)$ evaluated at the extrapolated value of $\tilde{\Phi}(x, t_0 + \Delta t)$ at the position sampled.

The second component of the $\partial B/\partial x$ source term arises due to the possibility of a discontinuity of $\Phi(x,t)$ at the zone edges, x_i, $i \in (1, N+1)$. This singular contribution to the $\partial B/\partial x$ source term is

$$-\frac{\mu c}{4\pi}\delta(x - x_i)(\phi_i^1(t_0 + \Delta t) - \phi_{i-1}^2(t_0 + \Delta t))$$

$$= -\frac{[2\mu]c\Delta t}{8\pi[\Delta t]}[\delta(x - x_i)](\phi_i^1(t_0 + \Delta t) - \phi_{i-1}^2(t_0 + \Delta t)) \qquad . \qquad (18)$$

As was the case for the continuous $\partial B/\partial x$ source, this source is handled with correlated particle pairs of equal and opposite weight and direction, with the positive μ particle being distributed according to 2μ. The distribution function for the time coordinate is $1/\Delta t$, The spatial distribution function is $\delta(x - x_i)$, where x_i is the location of the interface between zones, or an exterior zone with a problem boundary. The values, ϕ_0^2 and ϕ_{N+1}^1, where N is the number of zones, refer to the boundary conditions for the left and right hand side of the problem, respectively. There are $N + 1$ zone boundaries that contribute this source term.

6.2 Expanding T in the finite element basis functions

An alternative choice for handling the source terms is to expand the material temperature, T, in the finite element basis functions.

$$T(x,t) = \sum_{i=1}^{N} T_i(x,t) = \sum_{i=1}^{N}\sum_{l=1}^{L} T_i^l(x,t) = \sum_{i=1}^{N}\sum_{l=1}^{L} \mathrm{T}_i^l(t)\chi_i^l(x) \qquad (19)$$

This choice for the finite element expansion has the advantage that the material energy, assuming a constant specific heat during the time step, is linear. It is also likely that a second order spatial treatment of other physics, such as hydrodynamics, would be more easily coupled to our transport method if this choice for the expansion of the material temperature is used. The disadvantage is the complexity of sampling the radiation source strength that scales like T^4, and the resulting non-linear radiative coupling between zones. This will become clear in what follows.

Using the definition, $\Phi = aT^4$, and the expansion for the temperature in zone Z_i given by Eq. (19), we re-write the source terms within zone Z_i, again with the frequency dependence factored out.

$$-\frac{a}{4\pi}\frac{\partial(T_i(x,t))^4}{\partial t} = -\frac{a}{4\pi}\frac{\partial}{\partial t}\left(\sum_{l=1}^{L}\mathrm{T}_i^l(t)\chi_i^l(x)\right)^4$$

$$= -\frac{a}{4\pi}\frac{\partial}{\partial t}(\mathrm{T}_1^4\chi_1^4 + 4\mathrm{T}_1^3\mathrm{T}_2\chi_1^3\chi_2$$

$$+6\mathrm{T}_1^2\mathrm{T}_2^2\chi_1^2\chi_2^2 + 4\mathrm{T}_1\mathrm{T}_2^3\chi_1\chi_2^3 + \mathrm{T}_2^4\chi_2^4) \qquad (20)$$

In writing the last form of Eq. (20), we have suppressed the zone index, i, and have moved the basis function index, l, to a subscript position in order to make it less cumbersome to write the powers of the temperatures (functions of time) and the basis functions (functions of space). This notation will also be used in Appendix A.

As we did when expanding Φ in the basis functions, we use an implicit temporal treatment of the source terms. The time dependent coefficients jump from their value during the previous time step, $T(t_0)$, to their end of time step value, $T(t_0 + \Delta t)$, right at the beginning of the time step, leading to a Dirac delta function for the time derivative. Under this condition, Eq. (20) becomes:

$$-\frac{a}{4\pi}\frac{\partial(T_i(x,t))^4}{\partial t} = -\frac{a}{4\pi}\delta(t-t_0)\left\{(\mathrm{T}_1^4(t_0+\Delta t) - \mathrm{T}_1^4(t_0))\chi_1^4\right.$$

$$+4(\mathrm{T}_1^3(t_0+\Delta t)\mathrm{T}_2(t_0+\Delta t) - \mathrm{T}_1^3(t_0)\mathrm{T}_2(t_0))\chi_1^3\chi_2$$

$$+6(\mathrm{T}_1^2(t_0+\Delta t)\mathrm{T}_2^2(t_0+\Delta t) - \mathrm{T}_1^2(t_0)\mathrm{T}_2^2(t_0))\chi_1^2\chi_2^2$$

$$+4(\mathrm{T}_1(t_0+\Delta t)\mathrm{T}_2^3(t_0+\Delta t) - \mathrm{T}_1(t_0)\mathrm{T}_2^3(t_0))\chi_1\chi_2^3$$

14

$$+ (T_2^4(t_0 + \Delta t) - T_2^4(t_0))\chi_2^4\} \tag{21}$$

In the last manipulation, we convert to the normalized form of the spatial distribution functions for the source within the zone. Generalizing the notion expressed in Eq. (10), we rewrite Eq. (21) in terms of the normalized functions

$$\chi_1^4 = \frac{\Delta x}{5} \, \overline{\chi_1^4} \quad,$$
$$\chi_1^3 \chi_2 = \frac{\Delta x}{20} \, \overline{\chi_1^3 \chi_2} \quad,$$
$$\chi_1^2 \chi_2^2 = \frac{\Delta x}{30} \, \overline{\chi_1^2 \chi_2^2} \quad,$$
$$\chi_1 \chi_2^3 = \frac{\Delta x}{20} \, \overline{\chi_1 \chi_2^3} \quad,$$
$$\chi_2^4 = \frac{\Delta x}{5} \, \overline{\chi_2^4} \quad, \tag{22}$$

where Δx is the width of the zone. The result is

$$-\frac{a}{4\pi}\frac{\partial (T_i(x,t))^4}{\partial t} = -\frac{a\Delta x}{[2] \times 10\pi}[\delta(t - t_0)]\left\{(T_1^4(t_0 + \Delta t) - T_1^4(t_0))[\overline{\chi_1^4}]\right.$$
$$+ (T_1^3(t_0 + \Delta t)T_2(t_0 + \Delta t) - T_1^3(t_0)T_2(t_0))[\overline{\chi_1^3 \chi_2}]$$
$$+ (T_1^2(t_0 + \Delta t)T_2^2(t_0 + \Delta t) - T_1^2(t_0)T_2^2(t_0))[\overline{\chi_1^2 \chi_2^2}]$$
$$+ (T_1(t_0 + \Delta t)T_2^3(t_0 + \Delta t) - T_1(t_0)T_2^3(t_0))[\overline{\chi_1 \chi_2^3}]$$
$$\left. + (T_2^4(t_0 + \Delta t) - T_2^4(t_0))[\overline{\chi_2^4}]\right\} \quad. \tag{23}$$

We can now read off how to sample this source term. This source is uniform in μ, reflected in the distribution function, $1/2$, in the denominator, 20π. The temporal distribution function is $\delta(t - t_0)$, indicating that all of the source particles are born at the beginning of the time step. The numerical weight to be distributed among M sets of five particles is $-(a\Delta x)/(10\pi)$, with each member of a set of five particles receiving the weight $-(a\Delta x)/(10\pi M)$. Table 1 shows the unique characteristics of the members of a set of particles, namely their respective zone distribution functions and unknown factors.

As was the case in our discussion of the source terms for linear Φ in a zone, the frequency dependence of the source term is factored out using the chain rule before we decompose the strength of the source in terms of the spatial basis functions. The frequency distribution of the sampled particles is obtained from the finite difference form of $(4\pi/c)(\partial B/\partial \Phi)$, evaluated using the known temperature for the beginning of the time step, and the extrapolated temperature for the end of the time step, at the spatial position that was sampled for the particle. The details of sampling spatial positions within a zone, and sampling the frequency for a particle, are described in the Appendix.

15

Particle Number	Spatial Distribution Function	Unknown Factor
1	$\overline{\chi_1^4}$	$(\mathrm{T}_1^4(t_0 + \Delta t) - \mathrm{T}_1^4(t_0))$
2	$\overline{\chi_1^3 \chi_2}$	$(\mathrm{T}_1^3(t_0 + \Delta t)\mathrm{T}_2(t_0 + \Delta t) - \mathrm{T}_1^3(t_0)\mathrm{T}_2(t_0))$
3	$\overline{\chi_1^2 \chi_2^2}$	$(\mathrm{T}_1^2(t_0 + \Delta t)\mathrm{T}_2^2(t_0 + \Delta t) - \mathrm{T}_1^2(t_0)\mathrm{T}_2^2(t_0))$
4	$\overline{\chi_1^1 \chi_2^3}$	$(\mathrm{T}_1(t_0 + \Delta t)\mathrm{T}_2^3(t_0 + \Delta t) - \mathrm{T}_1(t_0)\mathrm{T}_2^3(t_0))$
5	$\overline{\chi_2^4}$	$(\mathrm{T}_2^4(t_0 + \Delta t) - \mathrm{T}_2^4(t_0))$

Table 1

A bundle of particles for the time derivative source terms in the expansion of T. Each member of the set of five particles has a unique spatial distribution functions and an associated unknown factor.

The continuous contribution to the $\partial B/\partial x$ source, in terms of the piecewise linear treatment of the temperature in a zone, is given by

$$
-\frac{\mu c a}{4\pi}\frac{\partial (T_i(x,t))^4}{\partial x} = -\frac{\mu c a}{4\pi}\frac{\partial}{\partial x}\left(\sum_{l=1}^{L}\mathrm{T}_i^l(t)\chi_i^l(x)\right)^4
$$

$$
= -\frac{\mu c a}{\pi}\left(\sum_{l=1}^{L}\mathrm{T}_i^l(t)\chi_i^l(x)\right)^3\frac{\partial}{\partial x}\left(\sum_{l=1}^{L}\mathrm{T}_i^l(t)\chi_i^l(x)\right) \quad . \quad (24)
$$

In our implicit temporal treatment, $\mathrm{T}_i^l(t)$ during the time step is $\mathrm{T}_i^l(t_0 + \Delta t)$. The space derivative of $\chi_i^2(x)$, within zone Z_i, is $1/(x_{i+1} - x_i)$. The space derivative of $\chi_i^1(x)$ has the opposite sign. This provides

$$
-\frac{\mu c a}{\pi(x_{i+1} - x_i)}\left(\sum_{l=1}^{L}\mathrm{T}_i^l(t_0 + \Delta t)\chi_i^l(x)\right)^3\left(\mathrm{T}_i^2(t_0 + \Delta t) - \mathrm{T}_i^1(t_0 + \Delta t)\right) \quad .(25)
$$

Again, suppressing the index i with the understanding that we are dealing with values associated with zone Z_i, moving the l index to a subscript position to avoid confusion with powers in the expansion of the temperature, and remembering that all temperature values are evaluated at the end of the time step, $(t_0 + \Delta t)$, we expand the sum,

$$
-\frac{\mu c a}{\pi \Delta x}\left(\mathrm{T}_1^3\chi_1^3 + 3\mathrm{T}_1^2\mathrm{T}_2\chi_1^2\chi_2 + 3\mathrm{T}_1\mathrm{T}_2^2\chi_1\chi_2^2 + \mathrm{T}_2^3\chi_2^3\right)(\mathrm{T}_2 - \mathrm{T}_1) \quad , \qquad (26)
$$

where Δx is the width of the zone.

Writing Eq. (26) in terms of the normalized functions

$$
\chi_1^3 = \frac{\Delta x}{4}\,\overline{\chi_1^3} \quad ,
$$

$$\chi_1^3 \chi_2 = \frac{\Delta x}{12} \, \overline{\chi_1^2 \chi_2} \quad ,$$

$$\chi_1^2 \chi_2^2 = \frac{\Delta x}{12} \, \overline{\chi_1 \chi_2^2} \quad ,$$

$$\chi_2^4 = \frac{\Delta x}{4} \, \overline{\chi_2^3} \quad , \tag{27}$$

and the distribution functions for the angular and time coordinates, we obtain

$$-\frac{[2\mu]ca\Delta t}{8\pi[\Delta t]} \left(\mathrm{T}_1^3 [\overline{\chi_1^3}] + \mathrm{T}_1^2 \mathrm{T}_2 [\overline{\chi_1^2 \chi_2}] + \mathrm{T}_1 \mathrm{T}_2^2 [\overline{\chi_1 \chi_2^2}] + \mathrm{T}_2^3 [\overline{\chi_2^3}] \right) (\mathrm{T}_2 - \mathrm{T}_1) \ . \tag{28}$$

At this point, we can read off the sampling scheme for the Monte Carlo treatment of this source term. The angular distribution function is 2μ. As was the case for our piecewise linear treatment of Φ, we deal with fact that the total source integrated over the range of μ is zero by sampling correlated particle pairs with equal and opposite weights in the $\pm\mu$ directions. In our Monte Carlo treatment of this source term, M sets of four particle pairs are created for each zone. The position coordinates for each of the four pairs in a set are sampled from $\{\overline{\chi_1^3}, \overline{\chi_1^2 \chi_2}, \overline{\chi_1 \chi_2^2}, \overline{\chi_2^3}\}$, and carry the unknown factors, $\{\mathrm{T}_1^3(\mathrm{T}_2 - \mathrm{T}_1), \mathrm{T}_1^2 \mathrm{T}_2(\mathrm{T}_2 - \mathrm{T}_1), \mathrm{T}_1 \mathrm{T}_2^2(\mathrm{T}_2 - \mathrm{T}_1), \mathrm{T}_2^3(\mathrm{T}_2 - \mathrm{T}_1)\}$, respectively. For a given pair, the particle sampled in the $+\mu$ direction has the numeric weight $-ca/8\pi M$, while the particle in the $-\mu$ direction has the opposite sign. For each space and time point sampled, the extrapolated value of the temperature is used in order to sample a frequency from $(4\pi/c)(\partial B/\partial \Phi)$.

If there is a discontinuity in $T(x,t)$ at the zone edges, x_i, $i \in (1, N+1)$, $\partial T^4(x,t)/\partial x$ has a singular contribution, again with the frequency dependence factored out, given by

$$-\frac{\mu ca}{4\pi} \delta(x - x_i) \left((\mathrm{T}_i^1(t))^4 - (\mathrm{T}_{i-1}^2(t))^4 \right) \quad , \quad i \in (1, N+1) \quad , \tag{29}$$

where $\mathrm{T}_0^2(t)$ is the boundary condition on the left surface of the slab, and $\mathrm{T}_{N+1}^1(t)$ is the boundary condition on the right. Identifying the angular, temporal and spatial distribution functions, and with our *implicit* differencing scheme that evaluates the temperatures at the end of time step values, the singular contribution to the $\partial B/\partial x$ source term becomes

$$-\frac{[2\mu]ca\Delta t}{8\pi[\Delta t]} \delta(x - x_i) \left((\mathrm{T}_i^1)^4 - (\mathrm{T}_{i-1}^2)^4 \right) \quad , \quad i \in (1, N+1) \quad , \tag{30}$$

where 2μ is the angular distribution function for the $+\mu$ particle of a $\pm\mu$ particle pair, $1/\Delta t$ is the distribution function for particles uniformly distributed across the time step, and $\delta(x - x_i)$ is the spatial distribution function indicating that the particle pairs are born on the zone interface, located at x_i. If

M particle pairs are sampled on each interface, the ones traveling in the $+\mu$ direction have a numeric weight of $-ca\Delta t/8\pi M$ and carry the unknown factor $((\mathrm{T}_i^1)^4 - (\mathrm{T}_{i-1}^2)^4)$, the difference in the fourth power of the temperature on each side of the interface. The frequency for the particles is sampled using the the finite difference form of $(4\pi/c)(\partial B/\partial \Phi)$, evaluated using the extrapolated end of time step temperatures for each side of the interface.

7 Galerkin treatment of the energy balance equation

In the prior section, we described how to deal with source particle sampling in the presence of unknown coefficients, whether they be the $\phi_i^l(t_0 + \Delta t)$ in the case of linear treatment of Φ in a zone (as a function of space), or the $\mathrm{T}_i^l(t_0 + \Delta t)$ in the case of linear treatment of T in a zone. Using the basis function representation of the source terms, correct spatial distributions can be established for Monte Carlo source particles whose weights have not yet been determined.

We must solve the energy balance equation, Eq. (2), in order to determine the unknown coefficients of the expansion of Φ, or T, at the end of the time step. The method of solving the material energy balance equation determines how we score energy deposition of the particles that get tracked in our Monte Carlo treatment of the transport equation, Eq. (1). To this end, we formally integrate the energy balance equation from t_0 to $t_0 + \Delta t$, bring the change in material energy to the right hand side, and refer to the result as the non-linear function $F(x)$, which must equal zero.

$$
\begin{aligned}
F(x) = {} & E_{mat}(T(x, t_0)) - E_{mat}(T(x, t_0 + \Delta t)) \\
& + 2\pi \int\limits_{t_0}^{t_0+\Delta t} dt \int\limits_0^{\infty} d\nu \int\limits_{-1}^{1} d\mu\, \sigma_a'(\nu, T(x, t_0)) D(x, t; \nu; \mu) \\
& + \int\limits_{t_0}^{t_0+\Delta t} dt\, G(x, t) \quad .
\end{aligned}
\tag{31}
$$

We would like to note that we are using $\sigma_a'(\nu, T(x, t_0))$, the opacity at the beginning of the time step, for the time integral of the difference field. In order to run the Monte Carlo solution to the transport equation, any absorption and scattering cross sections must be evaluated using temperatures from the beginning of the time step, $T(x, t_0)$, or a temperature that is extrapolated from the beginning of the time step, $\widetilde{T}(x, t)$.

$F(x)$ is a non-linear function of the $\phi_i^l(t_0 + \Delta t)$, or the $\mathrm{T}_i^l(t_0 + \Delta t)$, as the case

may be. If the unknown coefficients are the $\phi_i^l(t_0+\Delta t)$, the non-linearity occurs in the expression of the material energy. If the coefficients of the expansion are the $T_i^l(t_0 + \Delta t)$, the non-linearity occurs in the unknown factors in the time integral of $\sigma_a'D$. The local heating rate, G, is prescribed.

Generally, the function $F(x)$ is also a non-linear function of the position coordinate, x. Because of this we pursue a Galerkin treatment for the solution of $F(x) = 0$; we generate a set of algebraic equations to solve for the expansion coefficients, $\phi_i^l(t_0 + \Delta t)$ or $T_i^l(t_0 + \Delta t)$ as the case may be, by requiring that the projection of $F(x)$ onto the basis functions $\chi_j^k(x)$ defined by,

$$\mathrm{F}_j^k = \int dx\, \chi_j^k(x)\, F(x) \quad , \tag{32}$$

be zero. This restricts the solution, $T(x, t_0 + \Delta t)$ or $\Phi(x, t_0 + \Delta t)$, to be a piecewise linear function in the space spanned by the finite element expansion.

Identifying the terms in $F(x)$ from Eq. (31), we define:

$$E_j^k(t) = \int dx\, \chi_j^k(x)\, E_{mat}(x, t) \quad , \tag{33}$$

$$(\sigma D)_j^k = 2\pi \int dx\, \chi_j^k(x) \int\limits_{t_0}^{t_0+\Delta t} dt \int\limits_0^\infty d\nu \int\limits_{-1}^1 d\mu\, \sigma_a'(\nu, T(x, t_0)) D(x, t; \nu; \mu) \quad , \tag{34}$$

and

$$G_j^k = \int dx \int\limits_{t_0}^{t_0+\Delta t} dt\, \chi_j^k(x)\, G(x, t) \quad . \tag{35}$$

In terms of these definitions, we can write the algebraic system of equations we must solve as

$$\mathrm{F}_j^k = E_j^k(t_0) - E_j^k(t_0 + \Delta t) + (\sigma D)_j^k + G_j^k = 0 \quad . \tag{36}$$

The projection of the material energy at the start of the time step, $E_j^k(t_0)$, depends only upon known variables. The projection of the heat source during the time step, G_j^k, is prescribed. The projection of the material energy at the end of the time step, $E_j^k(t_0 + \Delta t)$, is non-linear when expressed in terms of the $\phi_i^l(t_0 + \Delta t)$ and linear when expressed in terms of the $T_i^l(t_0 + \Delta t)$. Additionally, it depends only upon the coefficients for basis functions in the same zone. The projection of the energy deposited from photon transport, $(\sigma D)_j^k$, is linear if the source terms are expressed in terms of the $\phi_i^l(t_0 + \Delta t)$ and non-linear

19

when the source terms are expressed in terms of the $T_i^l(t_0 + \Delta t)$. It also has a component that comes from the census particles from the prior time step that can be considered a boundary condition difference field at the start of the time step.

As noted above, and further exposited below, the system of algebraic equations, $F_j^k = 0$, is non-linear in its unknowns and we employ Newton-Raphson iteration for the solution. We start with a guess for the solution, the value of the dependent variables at the beginning of the time step, or some extrapolated value, and evaluate both F_j^k and the partial derivatives of F_j^k with respect to the unknowns at this starting point. We then solve a linear system for the error, producing a new value for the solution. This process is iterated until convergence is achieved. Our solution strategy, then, boils down to evaluating the projection of the material energy at the end of the time step, $E_j^k(t_0 + \Delta t)$, the projection of the absorbed energy, $(\sigma D)_j^k$, and their derivatives with respect to the unknown dependent variables at the trial values for the solution being refined using Newton-Raphson iteration.

We start with the material energy, in terms of the ϕ_i^l. Inverting $\Phi = aT^4$, we have $T = \Phi^{1/4}/a^{1/4}$. The energy density of the material, assuming a constant specific heat, c_v, and a constant material density, ρ, is

$$E(\Phi(x)) = \frac{\rho\, c_v}{a^{1/4}} \Phi^{1/4}(x) \quad . \tag{37}$$

In zone Z_i, $\Phi(x, t)$ is given by

$$\Phi_i(x, t) = \phi_i^1(t)\chi_i^1(x) + \phi_i^2(t)\chi_i^2(x) \quad . \tag{38}$$

The material energy density within the zone, then, is

$$E_i(x, t) = \frac{\rho\, c_v}{a^{1/4}} (\phi_i^1(t)\chi_i^1(x) + \phi_i^2(t)\chi_i^2(x))^{1/4} \quad , \tag{39}$$

and the total material energy is

$$E(x, t) = \sum_i E_i(x, t) \quad . \tag{40}$$

The projection of the material energy, defined above, is

$$E_j^k(t) = \int dx\, \chi_j^k(x)\, E(x, t) = \int dx\, \chi_j^k(x)\, E_j(x, t) \quad , \tag{41}$$

where the basis function χ_j^k selects $i = j$.

We find that the E_j^k may be evaluated, in terms of $\phi_j^1(t)$ and $\phi_j^2(t)$, in closed form,

$$\mathrm{E}_j^1(t) = \frac{\rho\,c_v}{a^{1/4}} 4\Delta x \Big(5\phi_1^{7/4} + 10\phi_1^{3/2}\phi_2^{1/4} + 15\phi_1^{5/4}\phi_2^{1/2} + 20\phi_1\phi_2^{3/4}$$
$$+ 16\phi_1^{3/4}\phi_2 + 12\phi_1^{1/2}\phi_2^{5/4} + 8\phi_1^{1/4}\phi_2^{3/2} + 4\phi_2^{7/4}\Big)$$
$$\Big/\Big(45(\phi_1^{1/4} + \phi_2^{1/4})^2(\phi_1^{1/2} + \phi_2^{1/2})^2\Big) \quad , \quad (42)$$

where Δx is the width of zone j. We have suppressed the common subscript, j, on the right hand side, have moved the basis function indices to the subscript in order to cleanly display the fractional powers. All of the ϕ are understood to be functions of time, t. $\mathrm{E}_j^2(t)$ is obtained by symmetry.

For the Newton-Raphson iteration of the solution, we require the partial derivative of $\mathrm{E}_j^1(t)$ with respect to ϕ_1 and ϕ_2. These, again, can be evaluated in closed form.

$$\frac{\partial \mathrm{E}_j^1(t)}{\partial \phi_1} = \frac{\rho\,c_v}{a^{1/4}} \Delta x \Big(5\phi_1^{3/2} + 15\phi_1^{5/4}\phi_2^{1/4} + 30\phi_1\phi_2^{1/2} + 50\phi_1^{3/4}\phi_2^{3/4}$$
$$+ 57\phi_1^{1/2}\phi_2 + 51\phi_1^{1/4}\phi_2^{5/4} + 32\phi_2^{3/2}\Big)$$
$$\Big/\Big(45(\phi_1^{1/4} + \phi_2^{1/4})^3(\phi_1^{1/2} + \phi_2^{1/2})^3\Big) \quad (43)$$

$$\frac{\partial \mathrm{E}_j^1(t)}{\partial \phi_2} = \frac{\rho\,c_v}{a^{1/4}} 4\Delta x \Big(\phi_1^{3/2} + 3\phi_1^{5/4}\phi_2^{1/4} + 6\phi_1\phi_2^{1/2} + 10\phi_1^{3/4}\phi_2^{3/4}$$
$$+ 6\phi_1^{1/2}\phi_2 + 3\phi_1^{1/4}\phi_2^{5/4} + \phi_2^{3/2}\Big)$$
$$\Big/\Big(45(\phi_1^{1/4} + \phi_2^{1/4})^3(\phi_1^{1/2} + \phi_2^{1/2})^3\Big) \quad (44)$$

$$\frac{\partial \mathrm{E}_j^2(t)}{\partial \phi_1} = \frac{\partial \mathrm{E}_j^1(t)}{\partial \phi_2} \quad\quad\quad\quad (45)$$

$$\frac{\partial \mathrm{E}_j^2(t)}{\partial \phi_2} = \frac{\partial \mathrm{E}_j^1(t)}{\partial \phi_1} \quad\quad\quad\quad (46)$$

The non-linearity of the material energy when we expand Φ in the basis functions is clear.

At the cost of a non-linear treatment of the source terms for the difference field, we can have a linear treatment of the material energy. Again, assuming

a constant specific heat, we have

$$E(T(x)) = \rho\, c_v T(x) \quad , \tag{47}$$

$$T_j(x,t) = \mathrm{T}_j^1(t)\chi_j^1(x) + \mathrm{T}_j^2(t)\chi_j^2(x) \quad , \tag{48}$$

and

$$E_j^1(t) = \rho\, c_v\, \Delta x\, \left(\frac{\mathrm{T}_j^1(t)}{3} + \frac{\mathrm{T}_j^2(t)}{6}\right) \quad , \tag{49}$$

where $E_j^2(t)$ is obtained by exchanging the basis function indices, 1 and 2, on the right hand side. Unlike the case with linear Φ, the linearity of the material energy expressed in terms of T allows one to cleanly separate the portion of the energy due to T_j^1 from the portion of the energy due to T_j^2. When the consistent projection of the material energy onto the χ_j^k generates trouble in the presence of steep gradients, we can lump the material energy on each end of the zone so that E_j^1 depends only upon T_j^1, and E_j^2 depends only upon T_j^2. This reduces the order of accuracy of the solution, but can be used to remove the monotonicity problem that would otherwise occur, thereby avoiding negative temperature solutions.

We are left with

$$(\sigma D)_j^k = 2\pi \int dx \int_{t_0}^{t_0+\Delta t} dt \int_0^\infty d\nu \int_{-1}^1 d\mu\, \chi_j^k(x)\, \sigma_a'(\nu, T(x,t_0)) D(x,t;\nu;\mu) \quad , \tag{50}$$

understanding that in addition to contributions from numeric (census) particles, contributions will come from symbolic particles carrying unknown factors involving $\phi_i^l(t_0 + \Delta t)$, or $\mathrm{T}_i^l(t_0 + \Delta t)$. In the case of a constant $\sigma_a'(\nu, T(x,t_0))$, as a function of temperature, the contribution of a particle track to the $(\sigma D)_j^k$ can be evaluated in closed form. In the case of a temperature dependent opacity, one might have to execute a multi-step numerical integration along the track, or use the first few terms of a power series expansion.

Formally noting the energy depositions from the different particle types when we are expanding the source terms in terms of the ϕ_i^l, the projection of the energy deposition can be written as

$$(\sigma D)_j^k = N_j^k$$

$$+ \sum_{i=1}^{N} \sum_{l=1}^{L} (DDT_i^l)_j^k \; (\phi_i^l(t_0) - \phi_i^l(t_0 + \Delta t))$$

$$+ \sum_{i=1}^{N} (DDX_i)_j^k \; (\phi_i^1(t_0 + \Delta t) - \phi_i^2(t_0 + \Delta t))$$

$$+ \sum_{i=1}^{N+1} (DELTA_i)_j^k \; (\phi_{i-1}^2(t_0 + \Delta t) - \phi_i^1(t_0 + \Delta t)) \quad , \tag{51}$$

where N_j^k is the contribution from census particles from the prior time step, $(DDT_i^l)_j^k$ is the contribution from $\partial/\partial t$ source particles born via $\overline{\chi}_i^l(x)$ in Eq. (16), $(DDX_i)_j^k$ is the contribution from $\partial/\partial x$ source particles born via Eq. (17), and $(DELTA_i)_j^k$ is the contribution from $\partial/\partial x$ source particles born via Eq. (18). In order to get the actual contribution to the energy deposition, these matrix elements must be multiplied by the appropriate unknown factors. The coefficients with out of range indices, $\phi_0^2(t_0 + \Delta t)$ and $\phi_{N+1}^1(t_0 + \Delta t)$, represent prescribed boundary conditions for the problem.

The structure of the energy deposition when expanding T in the finite element basis in order to generate the source terms is similar, expressed in terms of 10 different particle types and appropriate unknown factors.

7.1 Scoring a particle track

The $D(x, t; \nu; \mu)$ associated with a Monte Carlo particle track is

$$D_0 \, e^{-\sigma_a'(\nu)c(t-t_0)} \, \delta(x - x_0 - \mu_0 \, c \, (t - t_0)) \, \delta(\nu - \nu_0) \, \delta(\mu - \mu_0) \quad , \tag{52}$$

where D_0 is the weight of the particle at the start of the track and $(x_0, t_0; \nu_0; \mu_0)$ are the generalized coordinates of the particle at the start of the track, not the start of the time step. The track is made entirely within zone Z_j and within the time step. We are assuming for the purpose of this discussion that $\sigma_a'(\nu, T)$ is a constant function of temperature, but the discussion can be extended to cover the more complicated case.

The contribution of a particle track, defined in Eq. (52), to the term $(\sigma D)_j^k$, defined in Eq. (50), is calculated (modulo any unknown factor) by inserting the expression for the particle track into Eq. (50) and evaluating the integral. The integral over ν selects $\sigma_a'(\nu_0)$ and the integral over μ drops out trivially. The remaining delta function, enclosed in the integral over x, converts the x in the basis function to $x_0 + \mu_0 \, c \, (t - t_0)$, obtaining

23

$$\int\limits_{t_0}^{t_0+t'} dt\, c\, \sigma'_a(\nu_0)\chi^k_j(x_0 + \mu_0\, c\, (t - t_0))D_0 e^{-\sigma'_a(\nu_0)c(t-t_0)}$$

$$= \int\limits_0^{t'} dt\, c\, \sigma'_a(\nu_0)\chi^k_j(x_0 + \mu_0\, c\, t)D_0\, e^{-\sigma'_a(\nu_0)ct} \quad , \tag{53}$$

where $(t - t_0) \to t$.

For χ^1_j the result is

$$D_0 \frac{(\mu_0 + c\mu_0\sigma'_a(\nu_0)t + \sigma(\nu_0)(x_0 - x_{i+1}))}{\sigma'_a(\nu_0)(x_{i+1} - x_i)}e^{-\sigma'_a(\nu_0)ct} \;\Big|_0^{t'} \quad . \tag{54}$$

For χ^2_j the result is

$$D_0 \frac{(\mu_0 + c\mu_0\sigma'_a(\nu_0)t + \sigma(\nu_0)(x_0 - x_i))}{\sigma'_a(\nu_0)(x_{i+1} - x_i)}e^{-\sigma'_a(\nu_0)ct} \;\Big|_{t'}^0 \quad . \tag{55}$$

The sum is

$$D_0\, e^{-\sigma'_a(\nu_0)ct} \;\Big|_{t'}^0 \quad , \tag{56}$$

this being the weight lost by the particle during the track. The weight, D_0, may contain an unknown factor, leading to scoring the track in the appropriate matrix element.

8 Numerical results with a piecewise linear Φ

In presenting numerical results employing the piecewise linear treatment of Φ, our goal is to demonstrate the monotonicity problem that occurs in the presence of strong gradients [9] and to demonstrate the advantage for this expansion choice for problems near steady state. The basic test problem that we use for this demonstration is one where a finite slab is abruptly subjected to an incoming black body radiation flux on the left boundary while the right boundary radiates freely with no incoming radiation flux. Assuming that the incoming black body flux corresponds to a temperature higher than the initial material temperature, and with an initial radiation field that is in equilibrium with the material temperature, a thermal (Marshak) wave propagates from the left to the right and the problem eventually comes to steady state with a steady energy flow through the material.

In Figure 1 we show the results for such a problem. The gray opacity is one mean free path per cm and the specific heat of the material is given by $\rho c_v = 0.1$ jerk/cm^3 keV.[1] The initial temperature is $kT = 0.4$ keV and the slab is subjected to a $kT = 1$ keV black body applied on the left hand side at the start of the simulation. The time step size is 0.001 sh. With the dotted line, we show the material temperature at 0.03 sh using zones that are 1 cm in size, 5 zones for the problem. The solid line shows the 50 zone converged solution. The material temperature is discontinuous at zone boundaries, this being allowed by the finite element basis choice.

Two specific features of the 5 zone solution are notable. The first is that the curvature provided by the linear treatment of Φ is a poor fit for the leading edge of a Marshak wave, as demonstrated by comparison to the converged solution. The second is the relatively severe undershoot for the right side of the first zone, relative to the converged solution, occurring in spite of the fact that the energy deposited on this side of the zone is positive. This undershoot is a property of the finite zone size, not the finite time step size. It results from the self consistent solution of the material energy equation given the lopsided energy deposition in the first zone. The existence of the undershoot prevents us from running with a zero initial material temperature. The non-linearity of the material energy, when expressed in terms of Φ, makes it difficult to remove this pathology.

Although the monotonicity problem in the presence of steep gradients is a serious problem that limits the utility of this formulation, the linear treatment of Φ within a zone leads to a very accurate solution for problems near steady state where such steep gradients do not exist. In Figure 2 we show the solution for the problem defined above at a late time near steady state, again comparing the 5 zone solution to the converged 50 zone solution. Only the boundary layer at the right hand side of the slab is shown; it has one zone for the 5 zone solution and 10 zones for the 50 zone solution. The treatment of the boundary layer is fully converged with the 50 zone solution. In the interior of the slab, the 5 zone solution is in complete agreement with the 50 zone solution, reflecting the accuracy of the linear treatment of Φ for these physical conditions. In the first mean free path on the left hand side of the slab there is another boundary layer that is not shown in the figure.

9   Numerical results with a piecewise linear T

---

[1] Our units are 1 sh (shake) $= 10^{-8}$ sec, temperature measured in energy units, kT in keV, frequency measured in energy units, $h\nu$ in keV, and the material energy measured in jerks, 1 jerk $= 10^9$ Joules.

Given the monotonicity issue that has surfaced, we will now focus on the development of the piecewise linear treatment of the material temperature, T, in our remaining exposition. First, we repeat the problems run in Figures 1 and 2 so that we may compare, generally, the characteristics of the two choices for the material state variable, Φ and T. We will then show how lumping the material energy removes the monotonicity problem.

The results for the problem of Figure 1, which uses the finite element expansion of Φ, are repeated using the finite element expansion of T in Figure 3. Comparing Figures 1 and 3, we see that the converged 50 zone result is identical, and that the linear treatment of T in a zone provides a better match when compared to the converged solution for the leading edge of the Marshak wave. The linear treatment of T in the zone also tends to produce less undershoot on the back side of a zone in the presence of a strong gradient, although an undershoot is still present and must be dealt with.

The results for the problem of Figure 2, which uses an expansion of Φ as the linear material state variable, are repeated using T for the linear expansion in Figure 4. Comparing Figures 2 and 4, we see that the linear treatment of Φ does better, compared to the linear treatment of T, with small zone counts in near steady state conditions, although the second order accuracy provides for an accurate solution with only a modest increase in zone count.

The improved undershoot in the presence of strong gradients makes the linear treatment of T much more robust for time dependent problems, but it still suffers from the monotonicity problem. These undershoots will cause a negative temperature if the initial temperature in front of an advancing Marshak wave is low enough. The linear treatment of the material energy makes it possible to lump the material energy, regaining monotonicity in the presence of a strong gradient.

In Figure 5 we explore the effect of a lumped treatment of the material energy. We show the material temperature for the problem of Figure 3, except that the initial temperature is reduced to 0.2 keV and the result is shown at a slightly later time of 0.35 sh, adding results for a lumped material energy with the dotted line. The discontinuous solid line is the result without lumping The continuous solid line is the converged 50 zone solution. By lumping the material energy we make an error that causes the slope within a zone to be incorrect and yields a solution that is no longer second order accurate in space. In order to minimize any accumulated error due to lumping, we employ conditional lumping in problems we show later in this paper. In conditional lumping, we lump the material energy in a specific zone only during a time step where failing to lump would cause a negative temperature excursion.

10 Constraining the solution to be continuous

Our choice for the finite element basis expansion allows discontinuity in the material temperature at internal zone interfaces. The cost of allowing discontinuities is that we must deal with $2N$ unknowns where N is the number of zones in our one dimensional slab geometry setting. This can substantially increase the cost of the non-linear system solve and allow any undershoot to be worse than would occur if the left and right hand sides of an internal zone interface were constrained to agree. In this section we discuss, briefly, how to produce the solution corresponding to a basis that enforces continuity on the zone interfaces internal to the problem domain.

A basis function set that provides for a single temperature at each internal zone interface can be defined as follows.

$$
\begin{aligned}
\psi_1(x) &= \chi_1^1(x) \\
\psi_i(x) &= \chi_{i-1}^2(x) + \chi_i^1(x) \qquad (1 < i \leq N) \\
\psi_{N+1} &= \chi_N^2(x)
\end{aligned}
\tag{57}
$$

By expanding the material temperature in this basis, there are $N + 1$ coefficients for the expansion, these being the values of the material temperature on the zone interfaces, both internal and external.

The projections of $F(x)$ defined by Eq. (31) on the ψ_j can be obtained adding the appropriate F_j^k defined by Eq. (32). The partial derivatives of the projections of F on the ψ_j with respect to the unknown coefficients of the temperature expanded in the ψ_i basis are obtained by adding the derivatives with respect to the coefficients of the appropriate χ_i^l. The process boils down to a collapse of the $2N \times 2N$ problem to a $(N+1) \times (N+1)$ problem by adding the appropriate projections of F and the appropriate internal rows and columns of the Jacobian computed for the Newton-Raphson iteration. This obtains the solution for the ψ basis with a relatively local modification of the code used to compute the solution in terms of the χ basis. In addition, the dB/dx source particles associated with the internal discontinuities that are not allowed with the ψ basis need not be emitted as their weights will always be zero.

In Figure 6 we overlay the results of this treatment with the prior results of Figure 5. The undershoot at the right edge of the first zone is made less severe by the constraint of continuity, but this basis still suffers from the monotonicity problem unless lumping is used in order to avoid it.

11   Optically Thick Marshak Wave Problem

Up to this point we have explored the characteristics of a number of solution options using problems with an optical thickness of one mean free path per zone. The difference formulation reduces the Monte Carlo noise for optically thick problems, but our prior implementation, which used a piecewise constant treatment of the material temperature, forced calculations to be limited to roughly one mean free path per zone to avoid energy teleportation. In this section we explore the behavior of our piecewise linear implementation in the presence of optically thick zones.

Our test problem for this demonstration is, again, a Marshak wave problem with an initially cold medium. For the purpose of this demonstration, we use the continuous basis function set, with conditional lumping of the material energy using the piecewise linear treatment of the temperature. The incident radiation flux is applied to the left side of the problem as a 1 keV blackbody that is turned on at the start of the simulation. The gray opacity of the material is 200 mean free paths per cm, with a specific heat $\rho c_v = 0.1$ (jerk/cc keV) and a time step size of 0.01 sh.

In Figure 7 we show the material temperature at 30 sh for four instances of the problem, using 10, 20, 40 and 80 zones, respectively. The 10 zone case provides zones that are 100 mean free paths thick, scaling down to the 80 zone case that provides zones that are 12.5 mean free paths thick. The result for the piecewise linear treatment of the temperature, shown in Figure 7, is in sharp contrast to the behavior of the piecewise constant treatment of the material state variable, shown in Figure 8. The error in the piecewise constant solution scales roughly linearly with zone size, while the position of the leading edge of the Marshak wave for the piecewise linear treatment, neglecting the foot that must be the size of a zone, appears to be independent of the size of a zone. This is evidence that our extension of the SIMC method for the fully non-linear time dependent photon transport provides efficient and accurate calculations in the diffusion limit.

12   Discussion

We have extended the piecewise linear treatment of the material state variable for the Symbolic Implicit Monte Carlo (SIMC) transport method, originally developed by Clouet and Samba [6], to the case of the fully non-linear time dependent equations of photon transport, under conditions of local thermo-dynamic equilibrium (LTE), in the difference formulation. The use of the difference formulation removes two hurdles preventing practical application of

the method for the standard formulation of photon transport: the difficulty of sampling a transport source term that depends upon the material opacity at the location sampled, and the Monte Carlo noise that becomes an impasse when attempting to use the method in the diffusion limit.

In constructing a solution to the non-linear transport problem, one has the choice of linear treatment of the source terms and non-linear treatment of the material energy; or non-linear treatment of the source terms and linear treatment of the material energy. In implementing time dependent solutions for problems involving steep gradients, thermal or Marshak waves, we find that the monotonicity problem occurring in similarly treated heat flow problems also occurs for this method, and that the technique of lumping the material energy is effective in resolving the problem. We lump the material energy in only those zones and time steps where the consistent treatment of the material energy would produce a negative temperature excursion. This only occurs near the leading edge of a Marshak wave as it propagates through cold material. The need to lump the material energy in the presence of steep gradients produces a preference for a linear treatment of the material energy.

In addition to the original discretization method of Clouet and Samba, we have developed a method of enforcing continuity at the interfaces between interior zones; it is appropriate when the material opacity is not discontinuous. It reduces the number of variables that one must solve for and reduces the monotonicity problem, although it does not remove it.

In the results we have presented, time was discretized in an implicit piecewise constant manner, producing first order accuracy in the time integration. We have explored the use of temporal basis functions in an attempt to extend the accuracy of the time integration to second order. Although we do not show detailed results for this treatment of the time variable, we find that it is only conditionally stable in practice.

Our piecewise linear SIMC treatment of photon transport in the difference formulation produces exceptional performance in the diffusion limit, while offering seamless, accurate, treatment of optically thin portions of a problem. The propagation speed of a Marshak wave in optically thick media is independent of the zone size, while the piecewise constant SIMC treatment requires a per-zone optical thickness of less than one mean free path in order to produce a solution that is beginning to converge.

We have explored the properties of our piecewise linear SIMC treatment of the difference formulation for a constant opacity, as a function of temperature and frequency, and for static material without physical scattering. Because the source terms in the difference formulation are independent of the material opacity, they depend only upon the space and time derivatives of the

material temperature. The inclusion of a real material opacity only modifies the exponentiation and energy deposition of Monte Carlo particles as they are propagated, posing no additional difficulties for the source terms. The inclusion of physical scattering, likewise, poses no additional difficulty for the difference formulation.

The piecewise linear treatment of the difference formulation provides an accurate transport technique that is capable of robustly addressing problems in both optically thin, and optically thick, materials. It is capable of producing accurate transport solutions in the diffusion limit. An open question is whether or not the technique referred to as source tilting, that is used in the Implicit Monte Carlo (IMC) [11] method in order to improve the behavior of that algorithm for thick systems, can be used in the SIMC treatment of the difference formulation, and whether it will provide an equivalent performance in thick systems at a lower computational cost. We plan to explore this possibility in the future.

Acknowledgement

13   Appendix A: Spatial Sampling for Linear Temperature

As noted earlier, we now have multiple terms in the expansion of T in the finite element basis functions. These terms each have unique spatial distribution functions from which we wish to sample. According to [12], the standard model for sampling such a distribution function is:

(1) Integrate the probability density function (p.d.f) to obtain a cumulative distribution function (c.d.f.)
(2) Invert the c.d.f.
(3) Pass to this inverted c.d.f. a uniform random number between 0 and 1 in order to generate a value sampled according to the p.d.f.

Acknowledging that there are other approaches to sampling, for instance rejection techniques, this will be our plan of attack. We list the c.d.f.s of our normalized distribution functions below:

$$\frac{4}{\Delta x} \int_0^y \chi_1^3 dx = \frac{4y}{\Delta x} - \frac{6y^2}{\Delta x^2} + \frac{4y^3}{\Delta x^3} - \frac{y^4}{\Delta x^4} \quad , \tag{58}$$

$$\frac{12}{\Delta x} \int_0^y \chi_1^2 \chi_2 dx = \frac{6y^2}{\Delta x^2} - \frac{8y^3}{\Delta x^3} + \frac{3y^4}{\Delta x^4} \quad , \tag{59}$$

$$\frac{12}{\Delta x} \int_0^y \chi_1 \chi_2^2 dx = \frac{4y^3}{\Delta x^3} - \frac{3y^4}{\Delta x^4} \quad , \tag{60}$$

$$\frac{4}{\Delta x} \int_0^y \chi_2^3 dx = \frac{y^4}{\Delta x^4} \quad , \tag{61}$$

$$\frac{5}{\Delta x} \int_0^y \chi_1^4 dx = \frac{5y}{\Delta x} - \frac{10y^2}{\Delta x^2} + \frac{10y^3}{\Delta x^3} - \frac{5y^4}{\Delta x^4} + \frac{y^5}{\Delta x^5} \quad , \tag{62}$$

$$\frac{20}{\Delta x} \int_0^y \chi_1^3 \chi_2 dx = \frac{10y^2}{\Delta x^2} - \frac{20y^3}{\Delta x^3} + \frac{15y^4}{\Delta x^4} - \frac{4y^5}{\Delta x^5} \quad , \tag{63}$$

$$\frac{30}{\Delta x} \int_0^y \chi_1^2 \chi_2^2 dx = \frac{10y^3}{\Delta x^3} - \frac{15y^4}{\Delta x^4} + \frac{6y^5}{\Delta x^5} \quad , \tag{64}$$

$$\frac{20}{\Delta x} \int_0^y \chi_1 \chi_2^3 dx = \frac{5y^4}{\Delta x^4} - \frac{4y^5}{\Delta x^5} \quad , \tag{65}$$

and

$$\frac{5}{\Delta x} \int_0^y \chi_2^4 dx = \frac{y^5}{\Delta x^5} \quad . \tag{66}$$

We must now invert each of these functions. To do so, we employ Newton-Raphson iteration. This method converges very well, if given a good starting point. Our goal then is to find an approximation for the inverse of these functions that we can use as the starting point for the Newton-Raphson solver. This will allow us to sample these source terms using a single uniform random number, R, such that $0 \le R \le 1$.

13.1   The Method

We make three approximations for each of these functions, depending upon the value of R we choose. If R is small (near zero) or large (near one) we make appropriate approximations. If R is in neither of these regimes, we exploit the fact that these functions are nearly linear within this range. The transition

values between a "low," "medium" and "high" value of R are determined experimentally, by graphically displaying our first guess solutions and the actual function. As our goal is to reduce the number of iterations required by the numeric solver, we only need to find a sufficiently good first guess. It is important to note that two of these functions, Eq. (61) and Eq. (66) can be inverted trivially and do not require a numeric inversion. We take the fourth and fifth roots of the functions, respectively.

Furthermore, because the basis functions χ_1 and χ_2 are symmetric about a zone, these functions are also symmetric. This simplifies the matter, as we only need to uniquely sample for half of the functions. The other functions are sampled according to their symmetric counterparts. For instance, if we look at the left hand side of Eq. (62), we notice that all values for this function have symmetric counterparts in Eq. (66). If we sample Eq. (66) and subtract this value from the width of the zone, we obtain a properly sampled value for Eq. (62). By exploiting this symmetry we need to only focus on inverting three of these c.d.f.s. We choose to invert Eq. (60) and Eq. (65). As there is no symmetric counterpart to Eq. (64), our final choice is made for us. The method is identical for each of these functions. We will outline it in the context of Eq. (60) below.

13.2 Approximation for Small R

We begin by simplifying the notation so that our polynomial is easier to manipulate. Each time we pass our function a uniform random number, R, we return a position in space. So, we drop the normalization constants and let x be our sampled position. Therefore, Eq. (60) becomes:

$$R = 4x^3 - 3x^4 \quad . \tag{67}$$

We now let there be some function, $f(R)$, that satisfies the condition $R \cdot f(R) = 4x^3$. We know from Eq. (67) that:

$$
\begin{aligned}
R &= 4x^3 - 3x^4 \quad , &(68)\\
&= R \cdot f(R) - 3x^4 \quad , &(69)\\
&= R \cdot f(R) - \frac{3x}{4} R \cdot f(R) \quad . &(70)
\end{aligned}
$$

Now, when R is very small, so is x. We then disregard the higher-order term such that $R \approx 4x^3$ and invert this to get a value for x. Therefore, Eq. (70)

becomes:

$$R = R{\cdot}f(R) - \frac{3}{4}R{\cdot}f(R){\cdot}\left(\frac{R}{4}\right)^{\frac{1}{3}} \quad . \tag{71}$$

We can now solve for $f(R)$:

$$f(R) = \frac{1}{1 - \frac{3}{4}\left(\frac{R}{4}\right)^{\frac{1}{3}}} \quad . \tag{72}$$

Now, recall our goal is an initial guess for x to pass to the Newton-Raphson solver. Letting this guess be $x_\circ$, we know from above that $R{\cdot}f(R) = 4x_\circ^3$. We can now invert this relation and insert our value for $f(R)$:

$$x_\circ = \left(\frac{R}{4 - 3\left(\frac{R}{4}\right)^{\frac{1}{3}}}\right)^{\frac{1}{3}} \quad . \tag{73}$$

When R is sufficiently small, we pass the Newton-Raphson solver the initial guess of $x_\circ$ as given by Eq. (73) above.

13.3 Approximation for R Near One

When our value of R is close to one, we use a different approximation to obtain a value for $x_\circ$. We define new variables, d and y such that $R = 1 - d$ and $x = 1 - y$. Since both R and x are near one, d and y are very small. Let us take Eq. (67) and substitute our new values for R and x to get a function of d and y:

$$R = 4x^3 - 3x^4 \quad , \tag{74}$$
$$1 - d = 4(1 - y)^3 - 3(1 - y)^4 \quad . \tag{75}$$

Expanding and simplification yields:

$$d = 6y^2 - 8y^3 + 3y^4 \quad . \tag{76}$$

Because both y and d are small we drop the higher order terms and let $d \approx 6y^2$. Inverting yields:

$$y = \left(\frac{d}{6}\right)^{\frac{1}{2}} \quad . \tag{77}$$

We now have a guess for our $x_\circ$:

$$x_\circ = 1 - y = 1 - \left(\frac{d}{6}\right)^{\frac{1}{2}} = 1 - \left(\frac{(1-R)}{6}\right)^{\frac{1}{2}} \quad . \tag{78}$$

Equation 78 yields a first guess for the numerical solver given a value of R close to one.

13.4   Results

Figure 9 shows our first guess for $x_\circ$ plotted against the actual converged solution. Graphically we determined that our small R approximation is very good for values of R less than 0.2. Similarly, our near-one solution is good for values above 0.92. Within the region where neither of the discussed approximations is valid, we have made a linear fit to the curve. The equation of this line is $x_\circ = 55/99R + 0.31$. With these values for $x_\circ$, the Newton-Raphson solver converges typically within two or three iterations. Figure 10 shows a histogram of the normalized sampling of $\chi_1\chi_2^2$ using $100,000$ uniform random numbers between zero and one. The actual normalized function $(\chi_1\chi_2^2 = 12(-x^3 + x^2))$ is also plotted. It is clear that our sampling is accurate, to within sampling noise. As the number of random numbers increases, the histogram converges to the function. Our sampling of the other two functions, Eq. (64) and Eq. (65) is similar.

14   Appendix B: Improved Frequency Sampling

In the difference formulation, the source terms are derivatives of the Planck function. In the piecewise constant (in space) discretization there exist discontinuities in Φ both between zones and between time steps. In the piecewise linear (in space) discretization, Φ can still be discontinuous between zones, and in time, leading to the requirement for sampling $(4\pi/c)(\partial B/\partial \Phi)$ for finite differences. In the Appendix of [2] a rejection technique was used to sample the frequency distribution of these sources. Here, we develop an improved method, focusing on the $\partial B/\partial x$ source. The $\partial B/\partial t$ source is similar.

Let us assume that at some position $x = x_i$ the material state variable jumps from Φ_1 to Φ_2. Integrating the $\partial B/\partial x$ source in Eq. (6) shows that:

$$-\mu \int_{x_i-\epsilon}^{x_i+\epsilon} \frac{\partial B}{\partial x} dx = -\mu \left[B(\nu, (x_i + \epsilon)) - B(\nu, (x_i - \epsilon)) \right] \quad , \tag{79}$$

where ϵ is a small distance. Now, if we note that the material state variables to the left and right side of the discontinuity are Φ_1 and Φ_2 we can rewrite Eq. (79) as:

$$-\mu \int_{\Phi_1}^{\Phi_2} \frac{\partial B}{\partial \Phi} d\Phi = -\mu \left[B(\nu, \Phi_2) - B(\nu, \Phi_1) \right]. \tag{80}$$

Now we use the factorization of $B(\nu, \Phi) = (c/4\pi) b(\nu, \Phi) \Phi$, Eq. (5), to rewrite Eq. (80), obtaining

$$-\mu \int_{\Phi_1}^{\Phi_2} \frac{\partial B}{\partial \Phi} d\Phi = -\mu \frac{c}{4\pi} \left[b(\nu, \Phi_2)\Phi_2 - b(\nu, \Phi_1)\Phi_1 \right]$$

$$= -\mu \frac{c}{4\pi} \left[\frac{b(\nu, \Phi_2)\Phi_2 - b(\nu, \Phi_1)\Phi_1}{\Phi_2 - \Phi_1} \right] (\Phi_2 - \Phi_1) \quad . \tag{81}$$

Let us call the term in the brackets $f[\nu, \Phi_1, \Phi_2]$. We now show that $f[\nu, \Phi_1, \Phi_2]$ is a probability density function. For this, $f[\nu, \Phi_1, \Phi_2]$ must be strictly positive and integrate to unity for all frequencies.

The first condition is simple: $B(\nu, \Phi)$ is strictly monotonic in Φ. Namely, if $\Phi_2 > \Phi_1$, then $B(\nu, \Phi_2) > B(\nu, \Phi_1)$ for all values of ν. As such, the signs of the numerator and denominator of $f[\nu, \Phi_1, \Phi_2]$ will always match. Therefore, $f[\nu, \Phi_1, \Phi_2]$ will be positive for all values of ν.

To demonstrate the second condition, we integrate $f[\nu, \Phi_1, \Phi_2]$ over all frequencies:

$$\int_0^\infty f[\nu, \Phi_1, \Phi_2] d\nu = \int_0^\infty \left[\frac{b(\nu, \Phi_2)\Phi_2 - b(\nu, \Phi_1)\Phi_1}{\Phi_2 - \Phi_1} \right] d\nu$$

$$= \frac{1}{\Phi_2 - \Phi_1} \left[\int_0^\infty b(\nu, \Phi_2)\Phi_2 d\nu - \int_0^\infty b(\nu, \Phi_1)\Phi_1 d\nu \right] \quad . \tag{82}$$

Using Eq. (4), we get our result:

$$\int_0^\infty f[\nu, \Phi_1, \Phi_2] d\nu = \frac{1}{\Phi_2 - \Phi_1} [\Phi_2 - \Phi_1] = 1 \quad . \tag{83}$$

35

Therefore, $f[\nu, \Phi_1, \Phi_2]$ is a probability density function for frequencies.

We need a way to sample $f[\nu, \Phi_1, \Phi_2]$. If we rearrange Eq. (81) we get:

$$f[\nu, \Phi_1, \Phi_2] = \frac{1}{\Phi_2 - \Phi_1} \int_{\Phi_1}^{\Phi_2} \left[\frac{4\pi}{c} \frac{\partial B}{\partial \Phi} \right] d\Phi \quad . \tag{84}$$

This means that the frequency distribution for a finite jump across a boundary is an average of the term in the brackets in Eq. (84) over the jump in Φ. It can be found by Monte Carlo averaging over the interval in Φ. Our algorithm to do so employs a few steps:

(1) Sample a value of Φ uniformly on the interval $[\Phi_1, \Phi_2]$.
(2) From this Φ_{sample}, calculate the corresponding $T_{sample} = (\Phi_{sample}/a)^{1/4}$.
(3) Sample the term in the brackets of Eq. (84), returning a value for ν_{sample} according to this distribution. This is done using the method described in the Appendix of [2].

Figure 11 shows the results of our sampling of $f[\nu, \Phi_1, \Phi_2]$ plotted against the function $f[\nu, \Phi_1, \Phi_2]$ for different values of Φ_1 and Φ_2. There is excellent agreement between the sampling and the distribution function in all cases. Our histograms have been scaled to have unit area, whereas $f[\nu, \Phi_1, \Phi_2]$ is already normalized. In the case where $\Phi_1 = \Phi_2$, $f[\nu, \Phi_2, \Phi_1]$ is undefined. However, as described in the Appendix of [2],

$$\lim_{\Phi_1 \to \Phi_2} \frac{b(\nu, \Phi_1) \Phi_1 - b(\nu, \Phi_2) \Phi_2}{(\Phi_1 - \Phi_2)} = \frac{4\pi}{ca} \frac{\partial B(\nu, T)}{\partial T^4} \quad . \tag{85}$$

Thus, we plot the function $\frac{4\pi}{ca} \frac{\partial B(\nu,T)}{\partial T^4}$ against our histogram in the bottom right of Fig. 11. Our sampling algorithm does not change at all. This new method of sampling is both robust and accurate, handling all limiting cases. Our two temperatures, Φ_1 and Φ_2, can be close together, far apart, identical or zero. We need to neither employ a rejection technique nor check the ratio of the two temperatures to accurately sample the frequency distribution.

References

[1] A. Szőke, E.D. Brooks III, *The transport equation in optically thick media*, Journal of Quantitative Spectroscopy and Radiative Transfer **91** (2005), pp. 95-110.

[2] E.D. Brooks III, M.S. McKinley, F. Daffin, A. Szoke, *Symbolic Implicit Monte Carlo radiation transport in the difference formulation: a piecewise constant discretization,* Journal of Computational Physics **205** (2005), pp. 737-754.

[3] E.D. Brooks III, *Symbolic Implicit Monte Carlo*, Journal of Computational Physics **83** (1989), pp. 433-446.

[4] T. N'kaoua, *Solution of the nonlinear radiative transfer equations by a fully implicit matrix Monte Carlo method coupled with the Rosseland diffusion equation via domain decomposition*, SIAM J. Sci. Stat. Comput. **12** (1991), pp. 505.

[5] McKinley, M. S., Brooks, E. D, and Szoke, A., *Comparison of Implicit and Symbolic Implicit Monte Carlo Line Transport with Frequency Weight Vector Extension*, Journal of Computational Physics **189** (2003), pp. 330-349.

[6] Clouet, J.-F. and Samba, G. *Asymptotic diffusion limit of the symbolic Monte-Carlo method for the transport equation*, Journal of Computational Physics **195** (2004), pp. 293-319.

[7] B. Su and G.L. Olson, *Benchmark results for the non-equilibrium Marshak diffusion problem*, J. Quant. Spectr. Rad. Transfer **56** (1996) pp. 337-351 .

[8] G. Strang and G.J. Fix, *An analysis of the finite element method*, Prentice-Hall, 1973.

[9] Godunov, S. K., *A finite difference method for the computation of discontinuous solutions of the equation of fluid dynamics*, Mat. Sb. **47**, pp. 357-393.

[10] Frank Daffin, et al., *An Evaluation of the Difference Formulation for photon transport in a two level system*, Journal of Computational Physics **204** (2005), pp. 27-45.

[11] J.A. Fleck, Jr. and E.H. Canfield, *A Random Walk Procedure for Improving the Computational Efficiency of the Implicit Monte Carlo Method for Nonlinear Radiation Transport*, Journal of Computational Physics **54** (1984), pp. 508-523.

[12] M. H. Kalos and P. A. Whitlock, *Monte Carlo Methods*, John Wiley and Sons, New York, 1986.
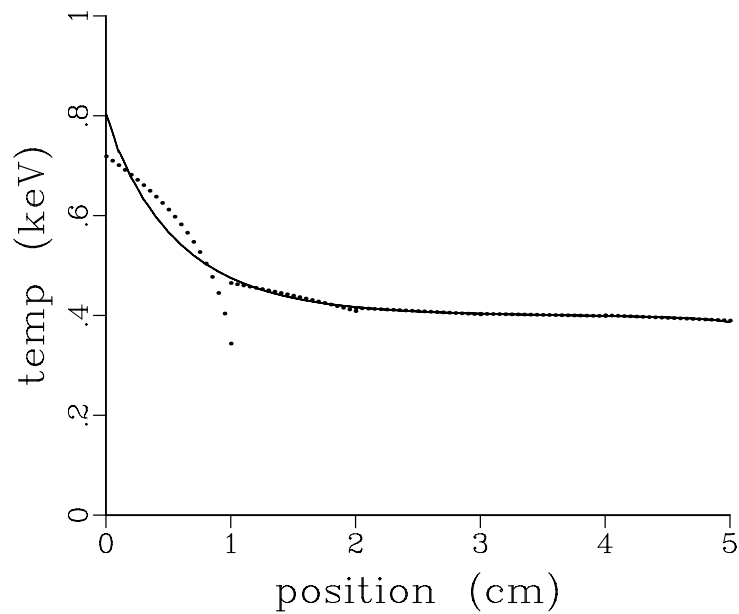
Fig. 1. A problem demonstrating the monotonicity issue, at a time $t = 0.03$ sh. The right hand side of the first zone has dropped below the initial temperature, $kT = 0.4$ keV, even though the energy deposited there has always been positive. The solid line shows the converged, 50 zone, solution. The dotted line shows the 5 zone solution. The solution for the temperature within the zone is curved because it is $\Phi = aT^4$ that is represented as a linear function within a zone.
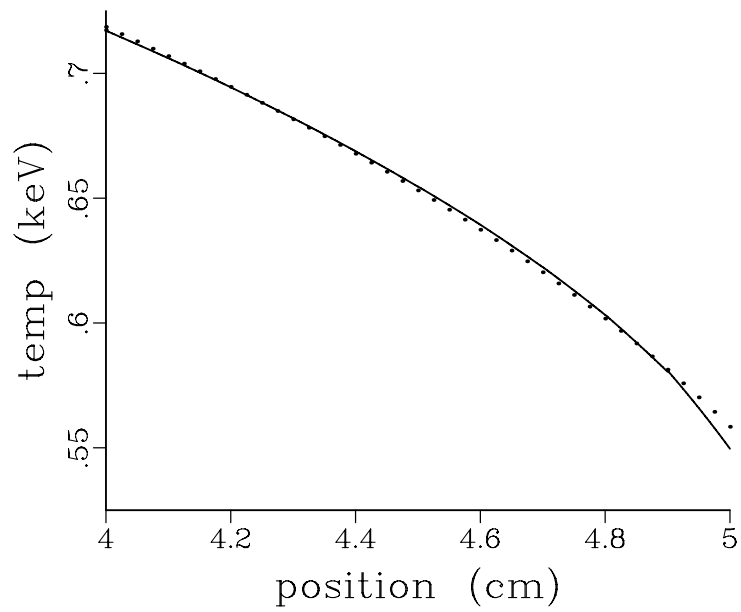
Fig. 2. The outer edge of the slab of the problem of Figure 1, one mean free path thick, shown at a late time near steady state. For the 5 zone discretization, the span from 4 to 5 cm is represented with one zone. This result is shown in the dotted line. For the 50 zone discretization, the same span is 10 zones, shown in the solid line. The small difference is the influence of the boundary layer.
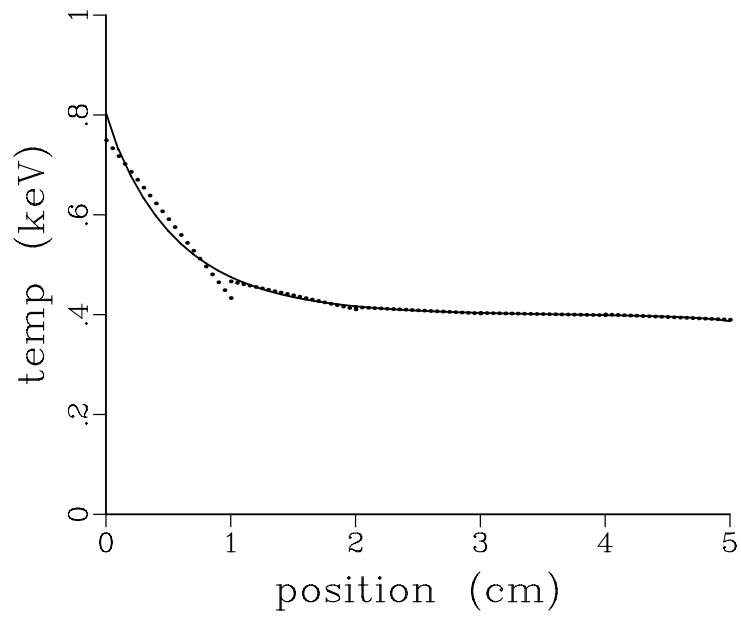
Fig. 3. A repeat of the calculation of Figure 1 using a linear expansion of T for the source terms. The dotted line is the 5 zone solution. The continuous line is the converged 50 zone solution.
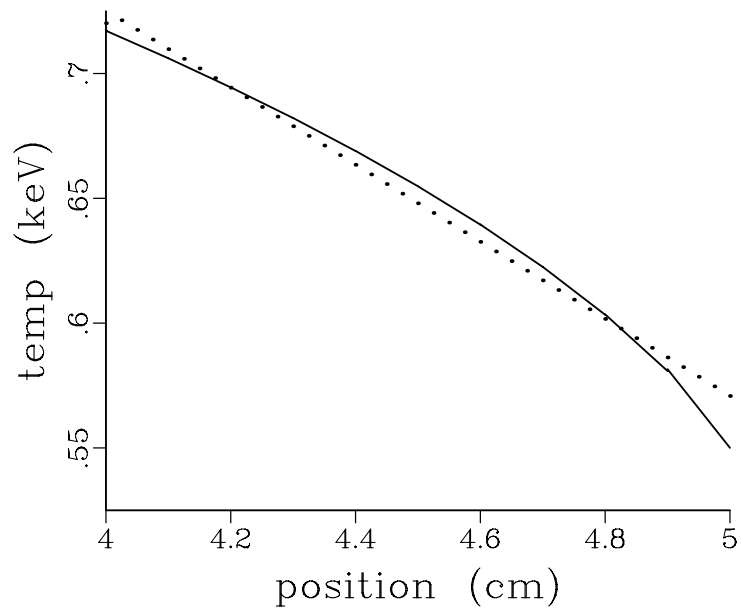
Fig. 4. A repeat of the calculation of Figure 2 using a linear expansion of T for the source terms. The dotted line is the 5 zone solution, one zone in the centimeter span shown. The solid line is the converged 50 zone solution.
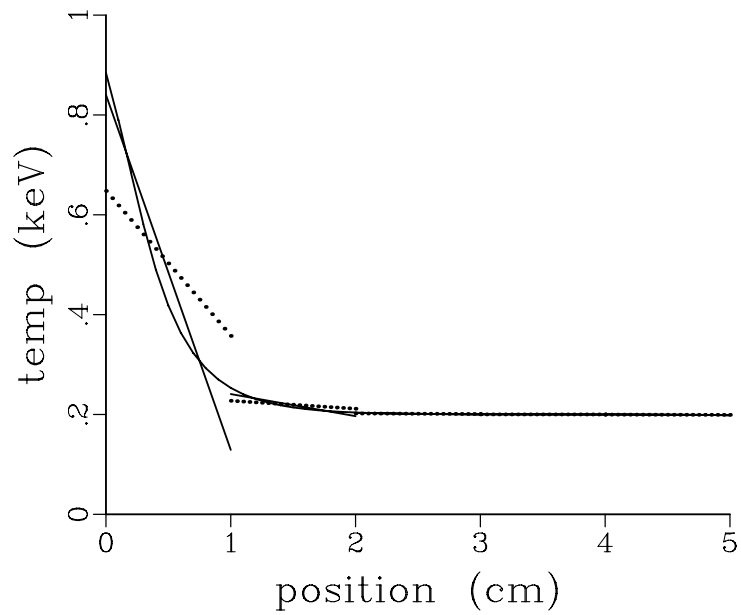
Fig. 5. A calculation showing the effect of continuous lumping. The time, $t = 0.035$ sh. The dotted line is for the 5 zone lumped case, with the discontinuous solid line not lumped. The solid continuous line is the converged 50 zone case.
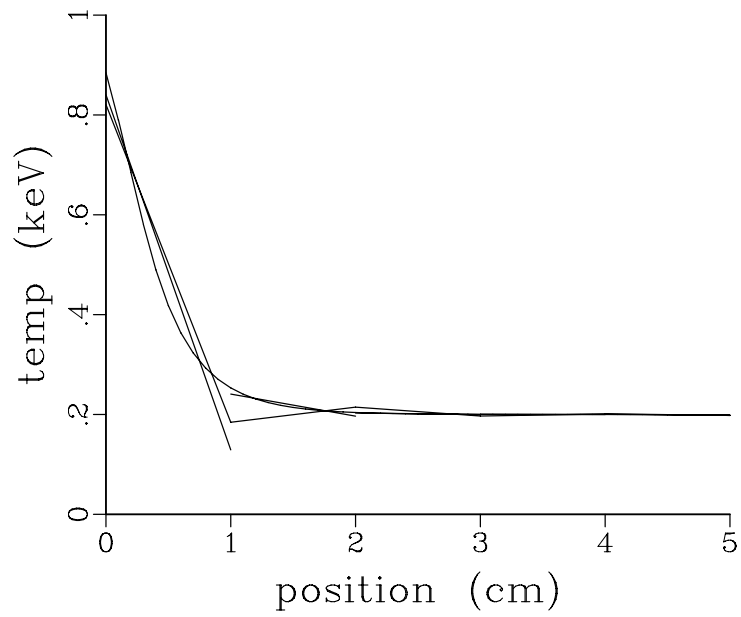
Fig. 6. A calculation showing the effect of enforcing continuity, at a time $t = 0.035$ sh. The basis for the discontinuous 5 zone solution is collapsed in order to produce the continuous 5 zone solution. The smooth curve is the converged 50 zone solution.
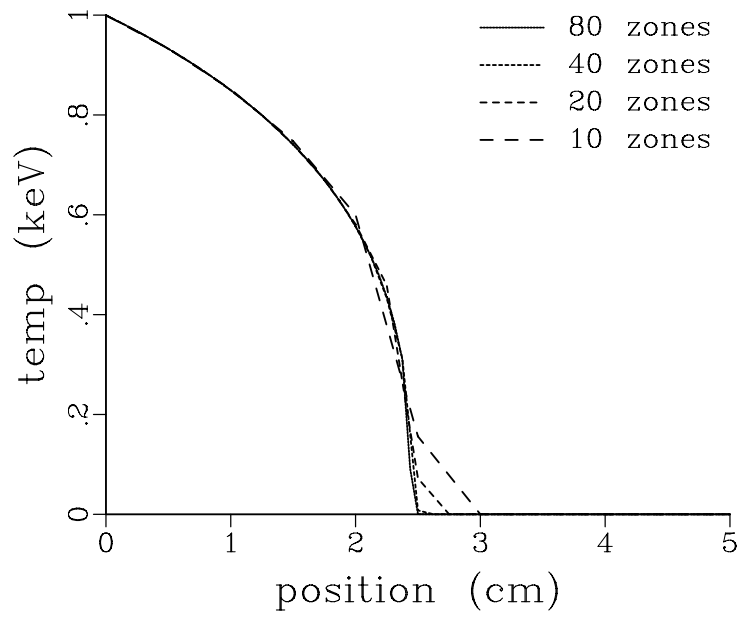
Fig. 7. Marshak wave problem, 200 mean paths per cm. The material temperature at a time $t = 30$ sh is shown. For our piecewise linear solution method, the speed of the wave is independent of the size of the zone.
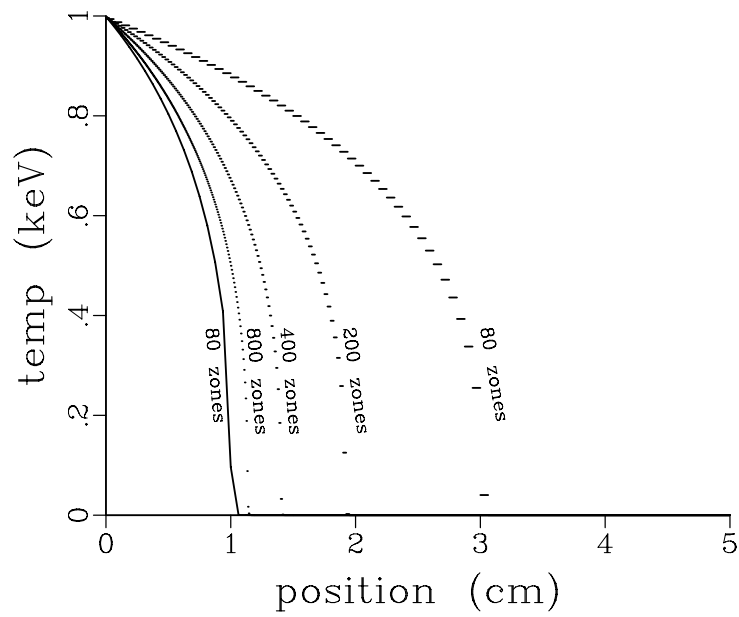
Fig. 8. A Marshak wave problem, 200 mean paths per cm, comparing the piece-wise constant implementation of the difference formulation to the piecewise linear implementation. The material temperature at $t = 5.0$ sh is shown. The piecewise constant curves are for 80, 200, 400 and 800 zone solutions, from the right to the left in the plot. The solid line is the 80 zone piecewise linear solution.
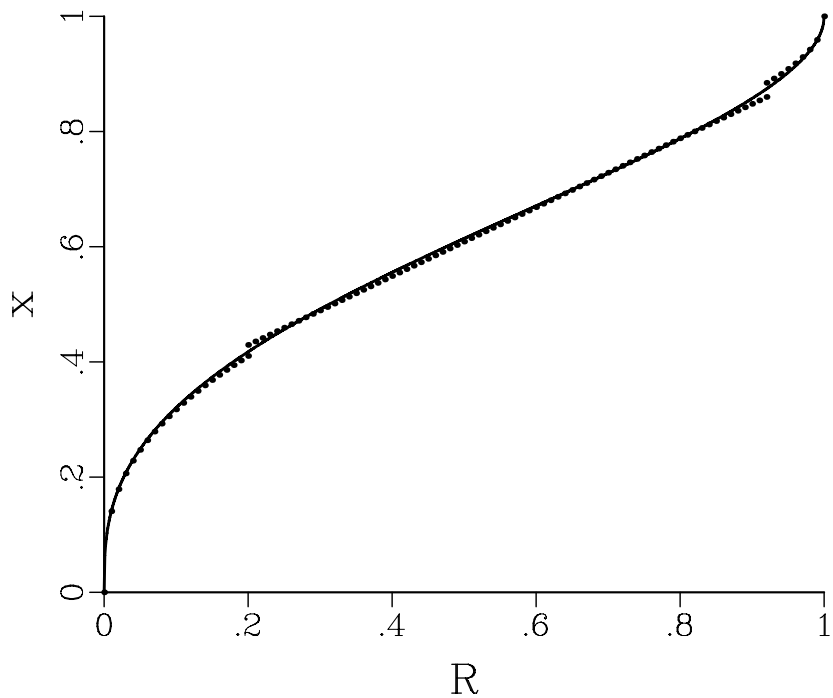
Fig. 9. The first guess solution for $x_\circ$ using our approximation techniques, shown with the black dots, over the converged c.d.f. shown with the solid black line. Our $x_\circ$ is treated differently depending upon the value of R chosen. For small and relatively large values of R, we use the solutions outlined in sections 13.2 and 13.3 respectively. Otherwise we approximate the function linearly.
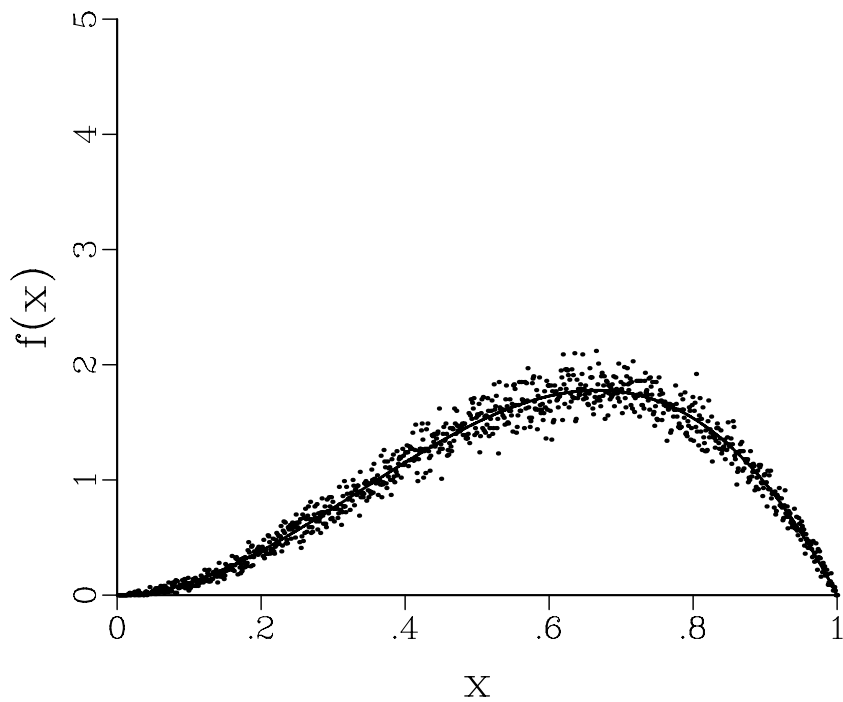
Fig. 10. Our normalized sampling of the function $\overline{\chi_1\chi_2^2}$ with $100,000$ random numbers plotted against the actual function. The zone width is taken to be one. The difference between the histogram and the actual function is from sampling error. As the number of uniform random numbers increases, the sampling converges to the function.
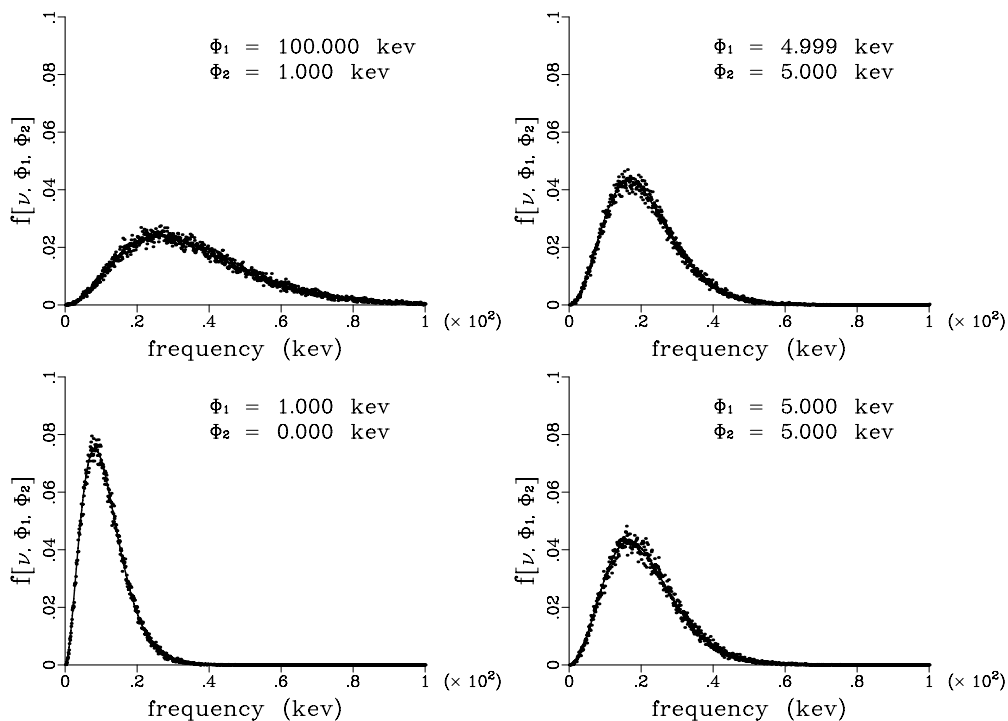
Fig. 11. Our normalized sampling of the function $f[\nu, \Phi_1, \Phi_2]$ with $100,000$ random numbers plotted against the actual function for varying values of Φ_1 and Φ_2. Our sampling is accurate when the two temperatures are close together or far apart, as shown in the upper right and upper left plots, respectively, regardless of whether Φ_1 or Φ_2 has the larger value. The bottom left plot shows accuracy when one temperature is zero. In this case, we are plotting $b(\nu, \Phi_1)$. When the two temperatures are identical, the drawn function is $(4\pi/ca)\partial B/\partial\Phi$. Even in this case, our histogram matches well.